© 2021. Published by The Company of Biologists Ltd | Development (2021) 148, dev188276. doi:10.1242/dev.188276

STEM CELLS AND REGENERATION

RESEARCH ARTICLE

Post-transcriptional regulation by the exosome complex is required for cell survival and forebrain development via repression of P53 signaling

Pauline Antonie Ulmke[1], Yuanbin Xie[1,2], Godwin Sokpor[1,3], Linh Pham[1,3], Orr Shomroni[4], Tea Berulava[5], Joachim Rosenbusch[1], Uttiya Basu[6], Andre Fischer[5,7,8], Huu Phuc Nguyen[3], Jochen F. Staiger[1] and Tran Tuoc[1,3,*]

ABSTRACT

Fine-tuned gene expression is crucial for neurodevelopment. The gene expression program is tightly controlled at different levels, including RNA decay. N^6-methyladenosine (m6A) methylation-mediated degradation of RNA is essential for brain development. However, m6A methylation impacts not only RNA stability, but also other RNA metabolism processes. How RNA decay contributes to brain development is largely unknown. Here, we show that Exosc10, a RNA exonuclease subunit of the RNA exosome complex, is indispensable for forebrain development. We report that cortical cells undergo overt apoptosis, culminating in cortical agenesis upon conditional deletion of Exosc10 in mouse cortex. Mechanistically, Exosc10 directly binds and degrades transcripts of the P53 signaling-related genes, such as Aen and Bbc3. Overall, our findings suggest a crucial role for Exosc10 in suppressing the P53 pathway, in which the rapid turnover of the apoptosis effectors Aen and Bbc3 mRNAs is essential for cell survival and normal cortical histogenesis.

KEY WORDS: Cortical development, RNA decay, Exosome complex, Exosc10, Apoptosis, P53 pathway, Aen and Bbc3

INTRODUCTION

The neocortex of the mammalian brain is radially structured into six neuronal layers and multiple functional domains that form the structural basis for sensorimotor processing and intellectual ability. In early cortical development, apical progenitors (APs) in the ventricular zone (VZ) function as neural stem cells (NSCs) and produce neurons via direct and indirect neurogenesis in a specific temporal order, which will make up the different cortical layers (Götz and Huttner, 2005; Kriegstein et al., 2006). In direct neurogenesis, APs divide asymmetrically to generate new APs and neurons. Neurons produced during early neurogenesis are distributed mainly in the lower cortical layers (LLs) L6 and L5. In indirect neurogenesis, APs divide to self-renew and produce basal progenitors (BPs) that undergo limited cycles of symmetric divisions to generate more neurons with upper layers (ULs) L4-L2 (Pontious et al., 2008).

Optimal regulation of gene expression is crucial for establishing the intricate balance between the rate of proliferation and differentiation of neural progenitor cells as well as cell viability and apoptosis. Transcriptional regulation plays a central role in controlling gene expression. However, regulation of gene expression is not limited to the transcriptional level. Post-transcriptional mechanisms, such as the regulation of RNA stability contribute in sharpening the expression of genes during development.

The evolutionarily conserved RNA exosome is an essential factor that modulates gene expression during development (Januszyk and Lima, 2014; Kilchert et al., 2016). The ring-like structured exosome complex contains 11 different exosome component (Exosc) subunits, including nine structural subunits (Exosc1-9) and two catalytic subunits (Exosc10, Dis3) (Januszyk and Lima, 2014; Kilchert et al., 2016). Together with structural counterparts, Exosc10 and Dis3 are able to degrade numerous RNAs using their ribonuclease activity. This makes the entire exosome complex indispensable for controlling the richness of RNAs, degrading malfunctional or mis-configured RNAs. The integrated Exosc subunits, which interact through composite surfaces with their co-factors, are essential for targeting the exosome to specific RNAs for degradation, therefore conferring functional specificity (Lubas et al., 2011; Januszyk and Lima, 2014; Kilchert et al., 2016; Lim et al., 2017; Puno and Lima, 2018; Schmid and Jensen, 2019).

Of note, mutations of the Exosc genes have been found in various human brain disorders, including corpus callosum hypoplasia, cerebellar atrophy, abnormal myelination, pontocerebellar hypoplasia with cerebellar and spinal motor neuron degeneration, and intellectual disability (Wan et al., 2012; Boczonadi et al., 2014; Di Donato et al., 2016; Burns et al., 2018; Morton et al., 2018; Fasken et al., 2020), suggesting important roles for the exosome complex in neural development.

To investigate the possible involvement of the exosome complex in brain development, we used a conditional knockout (cKO) of the RNA exonuclease subunit Exosc10 from early brain development in transgenic mice. Transcriptional profiling of the Exosc10cKO cortical tissue revealed that Exosc10 suppresses the expression of large sets of genes involved in various processes of brain development, including cell death-related pathways. RIP-seq and

[1]University Medical Center, Georg-August- University Goettingen, Goettingen 37075, Germany. [2]Department of Biochemistry and Molecular Biology, School of Basic Medical Science, Gannan Medical University, 341000 Ganzhou, The People's Republic of China. [3]Department of Human Genetics, Ruhr University of Bochum, Bochum 44801, Germany. [4]Microarray and Deep-Sequencing Core Facility, Georg-August- University Goettingen, Goettingen 37075, Germany. [5]German Center for Neurodegenerative Diseases, Goettingen 37075, Germany. [6]Department of Microbiology and Immunology, Vagelos College of Physicians and Surgeons, Columbia University, New York, NY 10032, USA. [7]Department for Psychiatry and Psychotherapy, University Medical Center, Georg-August-University Goettingen, Goettingen 37075, Germany. [8]Cluster of Excellence 'Multiscale Bioimaging: from Molecular Machines to Networks of Excitable Cells' (MBExC), University of Goettingen, Goettingen 37075, Germany.

*Author for correspondence (tran.tuoc@ruhr-uni-bochum.de)

Y.X., 0000-0003-3621-9920; T.T., 0000-0003-2079-7259

Handling Editor: Paola Arlotta
Received 16 January 2020; Accepted 29 December 2020

Development (2021) 148, dev188276. doi:10.1242/dev.188276

RNA degradation analyses uncovered that Exosc10 directly binds to and induces degradation of P53 signaling-related transcripts. Phenotypically, we found that elimination of Exosc10 leads to a massively enhanced apoptosis, reduced neurogenesis and dysgenesis of cortical layers, with the first effect being rescued by inhibition of P53 signaling. Overall, this study provides new insights into the post-transcriptional regulatory mechanism mediated by the RNA exosome complex, which acts upstream of P53 signaling in apoptosis suppression in brain development.

RESULTS

Expression of Exosc10 is indispensable for forebrain development and formation of cortical layers

Mutations in human Exosc2, Exosc3, Exosc8 and Exosc9 genes, and their associated brain disorders imply important roles for the exosome complex in neurodevelopment (Wan et al., 2012; Boczonadi et al., 2014; Di Donato et al., 2016). In further support of the involvement of the exosome complex in mammalian brain development, exosome genes are prominently expressed in the developing mouse cortex, especially in the ventricular zone (VZ) (Fig. 1A; Fig. S1A-J). Extracting the published scRNA-seq dataset of the mouse developing cortex (Telley et al., 2016) also confirmed the highest expression of exosome genes in apical progenitors (APs), which are found in the VZ (Fig. 1B; Fig. S1K-S). As Exosc10 is the exonuclease subunit of the RNA exosome complex (Fig. S1A), we aimed to study the role of Exosc10 in neural development by generating and characterizing the cortical phenotype of Exosc10 conditional knockout (cKO) mice.

To investigate the consequences of loss of Exosc10 in brain development, we bred mice bearing conditional inversion (COIN) alleles of Exosc10 (Economides et al., 2013; Pefanis et al., 2015) with different Cre lines, including telencephalon-specific *FoxG1*-Cre (Hébert and McConnell, 2000) and cortex-specific *Emx1*-Cre (Gorski et al., 2002), to generate the corresponding cKO mutants: cKO_*FoxG1*-Cre and cKO_*Emx1*-Cre. Telencephalon-specific cKO_*FoxG1*-Cre embryos exhibited an absolute absence of the telencephalon at E17.5 (Fig. S2A, arrow). To examine formation of the telencephalon at early stages, immunohistochemistry analysis was performed with antibodies against Sox2, Pax6, HuCD and NeuN in forebrain tissue of control and cKO_*FoxG1*-Cre embryos between E10.5 and E12.5 (Fig. S2B,C). The expression of these markers was found in telencephalon (Tel), diencephalon (Di) and mesencephalon (Mes) of control embryos, whereas their expression was seen only in Di and Mes structures in cKO_*FoxG1*-Cre mutants. This finding suggests that the deletion of Exosc10 at the onset of telencephalon formation in cKO_*FoxG1*-Cre embryos results in the failure of telencephalon formation, which makes this mouse line inappropriate for further investigations. At P6, the cortex in cKO_*Emx1*-Cre mice was significantly smaller than that of the control mice; however, we were still able to examine cortical development under Exosc10 deficiency (Fig. 1C,D).

The cKO mutants at P6 had visually smaller cortical size and thinner cortical layers than that of controls, as revealed by Satb2 immunostaining (Fig. 2A,G). To explore cortical layer formation in detail, we performed immunohistochemistry and evaluated the expression of cortical layer (L)-specific markers, such as reelin (L1; Fig. 2B), Cux1 (L2/3; Fig. 2C), Ctip2 (L5; Fig. 2D), Sox5 (L5/6; Fig. 2E) and Tbr1 (L6; Fig. 2F).

The population of reelin^{+} L1 neurons generated in the cortical hem and ventral telencephalon, where the Emx1 promoter is not active (Gorski et al., 2002), seems to be preserved in the cortex of cKO_Emx1-Cre mutants (Fig. 2B,G). In contrast, the numbers of Cux1^{+} L2/3, Ctip2^{+} L5, Sox5^{+} L5/6 and Tbr1^{+} L6 neurons, which are generated from cortical progenitors, were significantly reduced

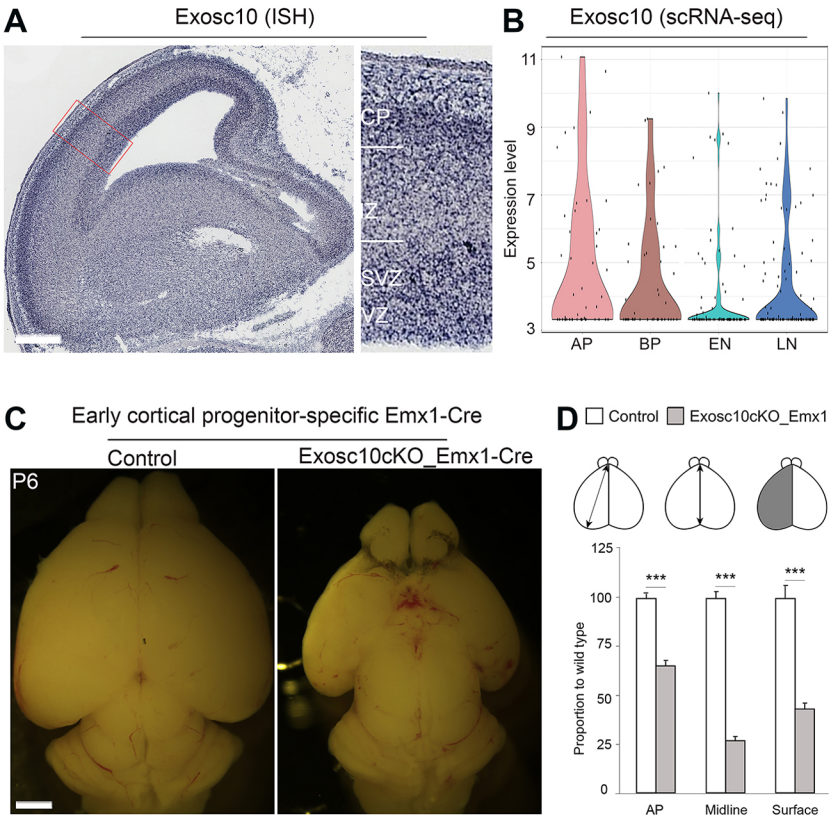

Fig. 1. The expression of Exsoc10 is indispensable for cortical development. (A,B) *In situ* hybridization analysis of sagittal sections obtained from GenePaint database (Visel et al., 2004) (A) and in scRNA-seq analysis (Telley et al., 2016) (B) of the E14.5 mouse cortex reveal that Exosc10 is widely expressed, with its highest level seen in apical progenitors (AP, in B) in the ventricular zone (VZ, in A). (C) At P6, the cortex in *dcKO_Emx1*-Cre mice is distinctly smaller than that of controls. (D) Quantification of the cortical proportions in *dcKO_Emx1*-Cre mice relative to control showing significant differences. AP, apical progenitors/RGCs; BP, daughter basal progenitors/IPCs; EN, early-born neurons; LN, late-born neurons; CP, cortical plate; SVZ, subventricular zone; VZ, ventricular zone. ***P<0.005. Scale bars: 1 mm.

Development (2021) 148, dev188276. doi:10.1242/dev.188276

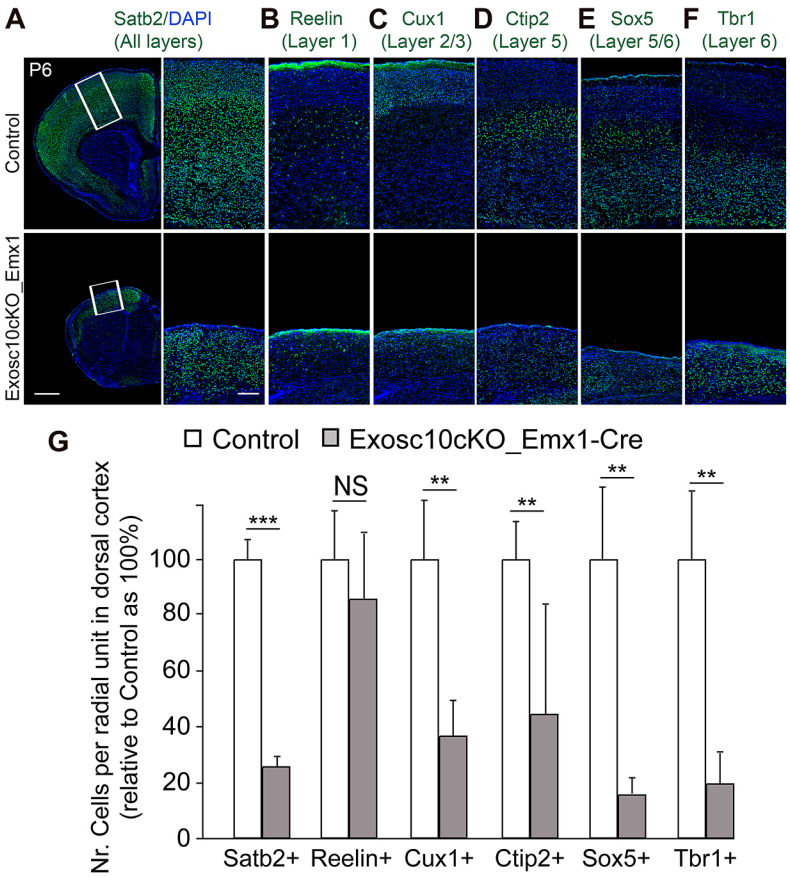

Fig. 2. Loss of neurons and a reduction in the thickness of cortical layers in postnatal Exosc10cKO mutants. (A-F) Immunohistochemistry showing cortical expression of neuronal markers specific for certain cortical layers: Satb2 (all layers, A), reelin (layer 1, B), Cux1 (layer 2/3, C), Ctip2 (layer 5, D), Sox5 (layer 5/6, E) and Tbr1 (layer 6, F) in coronal sections of Exosc10cKO and control at P6. Right images are higher magnifications of fields indicated by white frames. (G) Quantification of the neuronal markers in Exosc10cKO cortex at P6 relative to control. The cells were counted in the dorsal area at the rostral levels shown in A. $^{**}P<0.01$, $^{***}P<0.005$; NS, not significant. Scale bars: 1 mm and 200 µm (higher magnification).

in the cKO_Emx1-Cre cortex (Fig. 2C-G). Together, these results show that the expression of Exosc10 is required for normal forebrain development and cortical layer formation.

Exosc10 ablation in early cortical development causes massive apoptosis

The diminished population of neurons in the cKO cortex at postnatal stage promoted us to investigate the consequences of the loss of Exosc10 expression on neurogenesis at early embryonic stages. Consistent with the decreased number of neurons in cortical layers at P6 (Fig. 2), the Exosc10-ablated cortex at E13.5 displayed a diminished number of HuCD$^+$ and NeuN$^+$ neurons in cortical plate (CP) (Fig. 3A,B,D,E). Remarkably, the thickness of the germinal zones, i.e. the ventricular zone (VZ) and sub-ventricular zone (SVZ) (Fig. 3A-C), in the control cortex was comparable with that of the mutant cortex (Fig. 3A,B). Accordingly, the number of apical progenitors (Pax6$^+$ or Sox2$^+$) in VZ and basal progenitors (Tbr2$^+$) in SVZ was comparable in cKO and control cortices (Fig. 3A-E). These findings suggest that the deletion of Exosc10 might lead to an enhanced apoptosis or defect in neuronal differentiation in early cortical development, causing the observed brain microcephaly at the postnatal stage.

The immunohistochemical analysis with the apoptosis marker activated caspase 3 (Casp3) revealed that Exosc10 ablation engenders intense apoptosis in Exosc10cKO_Emx1-Cre cortex at E13.5, especially in the rostromedial area (Fig. 4A-C), where the Cre recombinase activity was found to be highest (Gorski et al., 2002; Narayanan et al., 2015; Nguyen et al., 2018). A dramatic increase in apoptosis was already evident in the mutant cortex at E11.5 (Fig. 4D). Apoptotic cells were observed in the entire mutant cortex, albeit more dominant in the basal side of cortical wall, suggesting that neurons were the most affected population of cells therein (Fig. 4A-C). Notably, there was no difference in the number of Casp3$^+$ apoptotic cells between control and Exosc10cKO cortices at postnatal stages, indicating that Exosc10 expression is required for cell viability only at embryonic stages of cortical development (Fig. S3).

Double immunohistochemical analyses of Casp3 and markers for apical progenitors (Sox2; Fig. 4A), basal progenitors (Tbr2; Fig. 4B) and neurons (NeuN; Fig. 4C) confirmed that apoptosis was found in all three cell populations in the cKO_Emx1-Cre cortex (indicated by filled arrows in Fig. 4A-C,E). Notably, the highest cell death rate was identified in NeuN$^+$ neurons (Fig. 4E). Altogether, our findings indicate that Exosc10 is crucial for cell viability in early cortical development.

Identification of Exosc10 target genes

To understand the molecular mechanisms underlying control of cortical development by Exosc10 and to identify the Exosc10 direct target transcripts, RNA sequencing (RNA-seq) as well as RNA immunoprecipitation sequencing (RIP-seq), were performed. In the RNA-seq, RNAs isolated from the E12.5 Exosc10cKO_Emx1-Cre and control cortices were sequenced (Fig. S4A,C). We found that loss of Exosc10 caused upregulation of 1031 genes and downregulation of 844 genes (adjusted $P<0.05$; Fig. 5A, Table S1). Gene ontology (GO) analysis of the upregulated genes reflected involvement of various brain development processes (Fig. 5B, Table S2). Consistent with the increased apoptosis, cell death-related pathways, such as regulation of apoptotic signaling pathway, and signal transduction by P53 mediators were upregulated in the cKO cortex (Fig. 5C, Table S2).

In our RIP-seq experiment, RNAs were purified from the E12.5 wild-type mouse cortex (Fig. S4B,D). By sequencing the

Development (2021) 148, dev188276. doi:10.1242/dev.188276

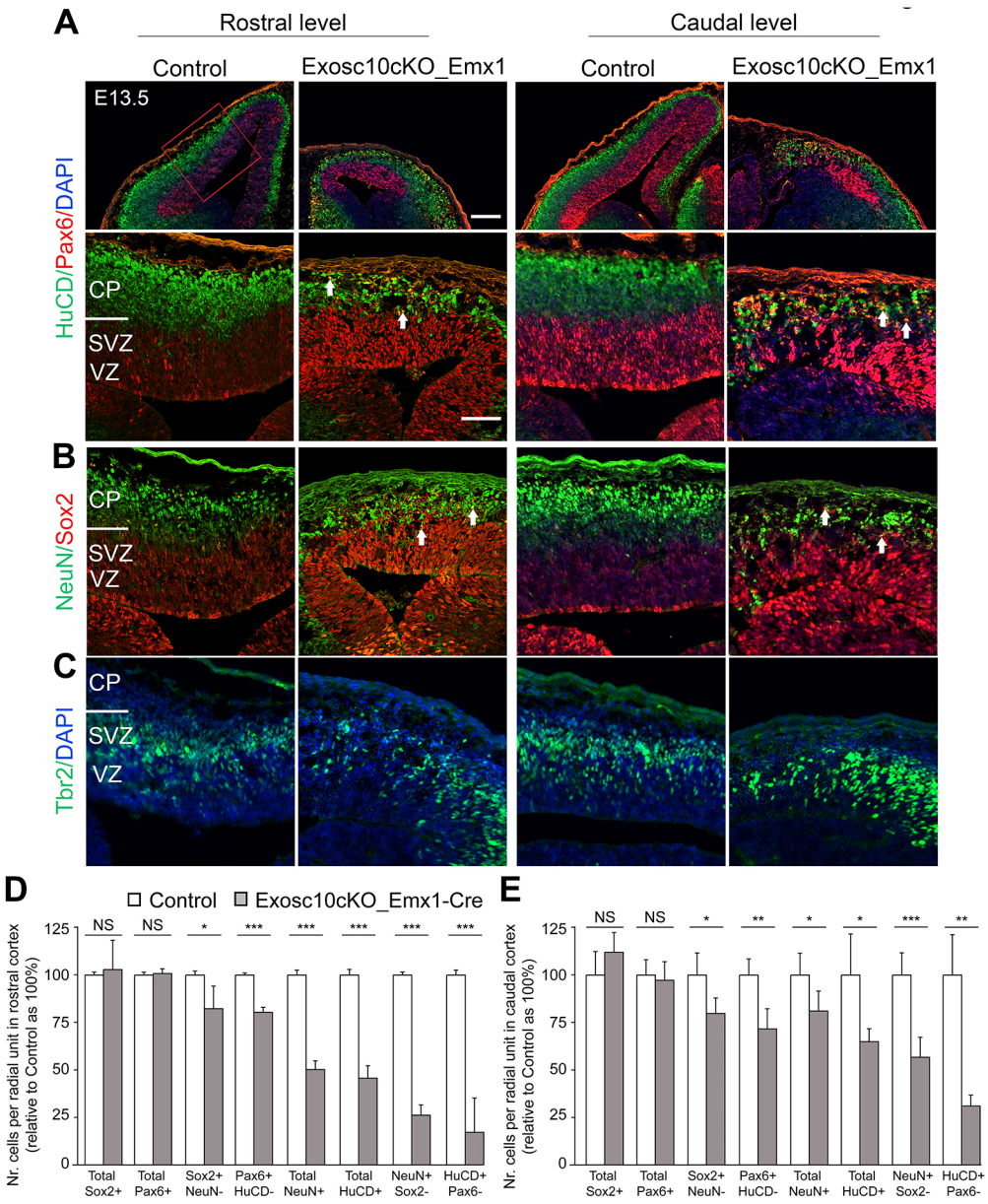

Fig. 3. A reduced thickness of the cortical plate but normal pools of cortical progenitors in Exosc10cKO cortex at E13.5. (A,B) Double immunohistochemical analyses with antibodies that specifically mark NSCs [Pax6 (A) and Sox2 (B)] and neurons [HuCD (A) and NeuN (B)] in the Exosc10cKO cortex and control at E13.5. For each, rostral and caudal sections are shown. Lower images are higher magnifications of fields indicated by the red frame. In cKO cortex, many Pax6$^+$ and Sox2$^+$ cells were also immunoreactive to HuCD and NeuN (A and B, white arrows). (C) Immunohistochemistry showing cortical expression of the intermediate progenitor marker Tbr2 in the E13.5 Exosc10cKO and control cortex. (D,E) Quantification of cells expressing neuronal progenitor genes (*Sox2* and *Pax6*) and neuronal genes [*NeuN* (*Rbfox3*) and *HuCD*(Elavl3/mHuC)] in the E13.5 cKO cortex relative to control at rostral (D) and caudal (E) levels. CP, cortical plate; SVZ, subventricular zone; VZ, ventricular zone. *P<0.05, **P<0.01, ***P<0.005; NS, not significant. Scale bars: 200 µm and 100 µm (higher magnification).

Exosc10-bound RNAs, binding enrichment of Exosc10 on 3159 transcripts was identified (adjusted P<0.05; Fig. 5B, Table S3). GO analysis revealed that the Exosc10-bound transcripts participate in various processes of brain development (Fig. 5D, Table S4). To identify candidates for functional analysis, we compared the RNAs upregulated in the Exosc10cKO cortex in RNA-seq experiment with transcripts bound by Exosc10 in RIP-seq analysis. We identified 144 transcripts common to the results of both experimental analyses (Fig. 5E, Table S5). Interestingly, those intersectional 144 upregulated genes showed an enrichment in the GO term ‘neuron death’ (Fig. 5F, Table S6).

In accordance with our immunohistochemical data showing increased numbers of Casp3$^+$ apoptotic cells, many genes involved in P53 apoptosis signaling (e.g. *Ccng1*, *Sesn2*, *Pmaip1*, *Bbc3* and *Aen*) were upregulated in the cortex of Exosc10cKO mutants (Fig. 5A; Fig. 6B). Furthermore, the results from our RIP-seq analysis revealed that transcripts of many apoptosis-related genes (e.g. Ccne1, Ccng2, Tsc2, Bbc3, Apaf1 and Aen) were bound by Exosc10 (Fig. 5B; Fig. 6A). Thus, our findings raise the possibility that Exosc10 inhibits apoptosis by directly suppressing expression of P53 signaling effector genes.

P53 pathway genes Aen and Bbc3 are direct targets of Exosc10 in the developing cortex

Among the transcripts belonging to the P53 pathway, Aen (apoptosis enhancing nuclease) and Bbc3 (BCL2 binding component 3; also known as PUMA, P53-upregulated modulator of apoptosis) were bound by Exosc10 (Fig. 6A). Their upregulated expression in the Exosc10cKO cortex was first revealed by RNA-seq (Fig. 6B), then confirmed by qPCR (for Bbc3, Aen and Atr; Fig. 6C) and immunohistochemical analyses (for Aen; Fig. 6D,E), making them strong candidates for mediating regulation of apoptosis by Exosc10.

To ascertain the functional effect of Exosc10 binding, we examined whether Exosc10 deletion influences decay of these identified transcripts. For this purpose, an RNA degradation assay was performed using cultured cortical NSCs derived from E12.5 Exosc10 COIN/COIN embryos. NSCs were treated with either

Development (2021) 148, dev188276. doi:10.1242/dev.188276

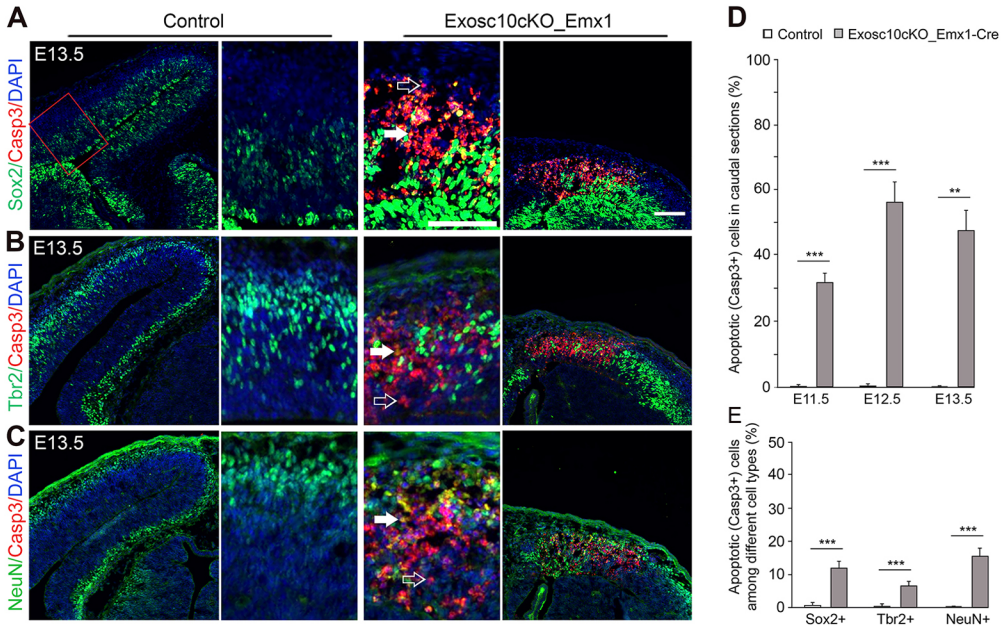

Fig. 4. Exosc10 ablation in early cortical progenitors causes massive apoptosis. (A-C) Double immunohistochemical analyses for the apoptosis marker activated caspase 3 (Casp3) together with Sox2 for NSCs (A), Tbr2 for IPs (B) or NeuN for neurons (C) in the Exosc10cKO cortex and control at E13.5. Middle images are higher magnifications of fields indicated by the red frame. White arrows indicate cells co-expressing Casp3 and the cell type marker; empty arrows indicate cells expressing only Casp3. (D) Quantification of apoptotic cells in Exosc10cKO cortex and control at E11.5, E12.5 and E13.5. (E) Quantification of apoptosis in different cell types by counting Casp3$^+$ cells among Sox2-, Tbr2- or NeuN-expressing cells in the E13.5 cKO and control cortex. CP, cortical plate; SVZ, subventricular zone; VZ, ventricular zone. ***P*<0.01, ****P*<0.005; NS, not significant. Scale bars: 200 µm and 100 µm (higher magnification).

soluble Tat-Cre recombinase to knockout Exosc10 (Exosc10KO) or vehicle as a control group (Fig. 6F; Fig. S5). An actinomycin D-based method was used to halt *de novo* transcription (Yoon et al., 2017). The cells were harvested and qPCR was performed to quantify the transcript level of Aen and Bbc3 in cultured NSCs before (0 h) and after 5 h and 17 h treatment of actinomycin D (Fig. 6F). Compared with control, a higher stability of Aen transcripts in Exosc10KO NSCs was observed after 5 h and 17 h treatment of actinomycin D (Fig. 6G). The higher RNA stability of Bbc3 in mutant NSCs than that in controls was seen after 17 h of actinomycin D treatment (Fig. 6H). These results indicated that Exosc10 directly binds and degrades transcripts of Aen and Bbc3.

To consolidate our observation that Exosc10 may regulate apoptosis via suppression of the P53 apoptosis pathway, *in vivo* rescue experiments were performed. We used a P53 inhibitor, pifithrin-α (PFTα), that is known to inhibit P53-dependent activation of P53-targeted genes (Komarov et al., 1999). PFTα was injected daily starting from 9.5 days post coitum (d.p.c.), and the PFT-treated Exosc10cKO animals were examined at E13.5 (Fig. 7A). Whereas 52.0±3.5% of cells in the PFT-untreated (non-injected) Exosc10cKO cortex were apoptotic, the percentage of Casp3$^+$ cells decreased to 31.0±9.2% upon PFTα treatment (Fig. 7B,C). Thus, the observed apoptotic phenotype in Exosc10cKO mutants was largely rescued by inhibition of the P53 pathway in the developing cortex. Among the P53 pathway-related genes, we compared the expression of *Bbc3* and *Aen* from control and cKO cortices, which were treated with either vehicle or P53 inhibitor. Remarkably, PFTα treatment does not significantly rescue the aberrant upregulation of Aen upon the loss of Exosc10 in the developing cortex (Fig. 7D). Treatment with PFTα, however, decreases the expression of Bbc3, which is upregulated in cKO cortex (Fig. 7E). This is in line with the evidence that Bbc3 (but not Aen) is a direct target of P53, as the promoter region of Bbc3 contains P53-binding sites and can be directly activated by P53 (Han et al., 2001).

To address whether Exosc10 regulates cortical development partly via suppression of P53 signaling, pregnant mice between 9.5 and 15.5 days post coitum (d.p.c.) were intraperitoneally injected daily with PFTα solution. Owing to the perinatal lethality of PFTα-treated animals, the brain samples were collected at E18.5 for phenotype analysis (Fig. 8A). The expression of Satb2, which marks the majority of projection neurons in all cortical layers and areas (Alcamo et al., 2008; Britanova et al., 2008), was then examined in control, and in cKO with and without PFTα treatment. The treatment with P53 inhibitor did not influence the size of wild-type (control) cortex, as indicated by Satb2 expression. Remarkably, when compared with vehicle-treated cKO embryos, PFTα-treated embryos had a significantly larger cortex. Concurrently, PFTα administration in cKO mutants resulted in an increase in the number of Satb2$^+$ neurons (Fig. 8B-F). The findings indicate that treatment with the P53 inhibitor partly rescues the aberrant cortical morphology in mutants.

Altogether, these results reveal that loss of Exosc10 during early cortical development causes aberrantly enhanced expression of P53 pathway-related transcripts such as Aen and Bbc3, and causes increased apoptosis similar to that observed after P53 overexpression (Fig. 8G). These findings demonstrate that the balance between the RNA exosome complex and P53 signaling activity is essential for cell survival and for normal cortical development (Fig. 8G).

DISCUSSION

Here, we have investigated the possible function of the RNA exonuclease Exosc10 in brain development. We demonstrate that

Development (2021) 148, dev188276. doi:10.1242/dev.188276

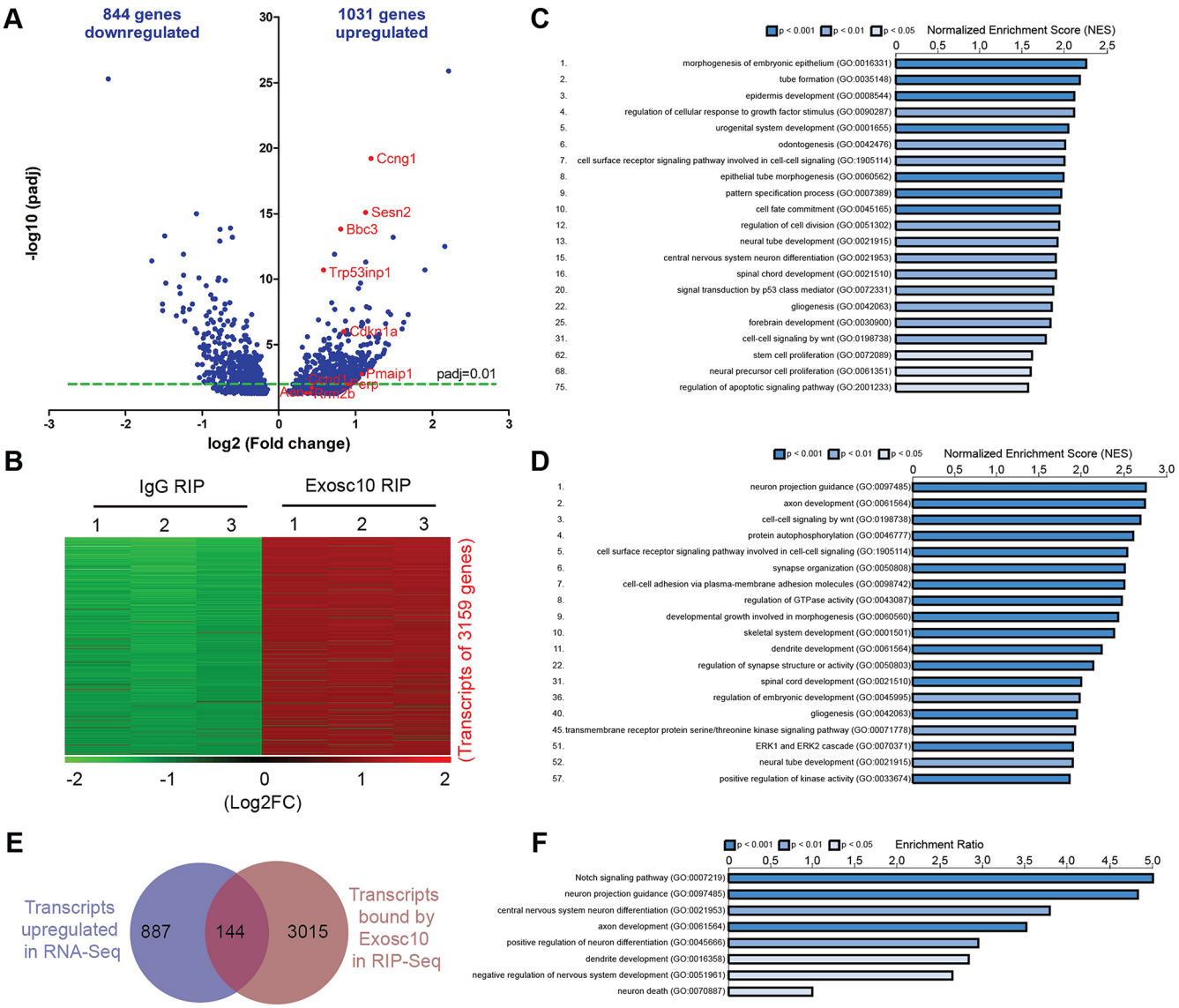

Fig. 5. Exosc10 controls global gene expression in early cortical development. (A,B) Volcano plot and heatmap showing significant changes in gene expression (A) and transcript-binding enrichment (B) revealed by RNA-seq (E12.5 Exosc10cKO cortex versus control) and RIP-seq (E12.5 cortex, Exosc10 antibody versus IgG) analyses, respectively. (C,D) Gene ontology analysis of genes upregulated in RNA-Seq (C) and transcript-binding enrichment in Exosc10 RIP-Seq (D). (E) The overlap between upregulated genes in RNA-Seq of E12.5 Exosc10cKO cortices and transcript-binding enrichment in Exosc10 RIP-Seq. (F) Gene ontology analysis of upregulated genes in RNA-Seq and their transcript bound by Exosc10 in RIP-Seq.

expression of Exosc10 is crucial for controlling cell survival and cortical development. Our findings indicate that Exosc10 performs an essential function in controlling P53-mediated apoptosis signaling by directly degrading the P53 signaling-related transcripts such as Aen and Bbc3 (Fig. 8G).

Emerging roles of RNA stability regulation in brain development

Post-transcriptional regulations such as RNA modification and RNA stability are emerging as mechanisms that are essential for regulation of gene expression. The best known mechanism of RNA modification, so far, is the methylation of nitrogen 6 in adenosine (N6-methyladenosine, m6A). The m6A writer complex, consisting of Rbm15, Wtap, Mettl3 and Mettl14, is responsible for addition of methyl groups to RNA (Liu et al., 2014; Wang et al., 2016). On the other hand, the m6A eraser Alkbh5 can remove methyl groups installed on RNA (Zheng et al., 2013). YTH proteins and eIF3 can serve as m6A readers to recognize m6A (Meyer et al., 2015; Patil et al., 2016). Recent studies suggest important roles for m6A methylation in the modulation of RNA stability in brain development (Yoon et al., 2017; Li et al., 2018; Wang et al., 2018; Widagdo and Anggono, 2018; Flamand and Meyer, 2019).

m6A deficiency by Mettl14 cKO in the developing mouse brain increased the stability of NSC transcripts, causing lengthening of the cell cycle of NPCs and prolongation of cortical neurogenesis further at postnatal stage (Yoon et al., 2017). The m6A depletion by Mettl14 cKO also changed the levels of modified histones and of transcripts encoding histone-modifying enzymes, indicating that m6A-dependent control of epigenetic program alterations is involved in neurodevelopment (Wang et al., 2018).

Deletion of m6A reader Ythdf2 in Ythdf2 KO mice leads to late embryonic lethality. Neurogenesis was declined significantly with

Development (2021) 148, dev188276. doi:10.1242/dev.188276

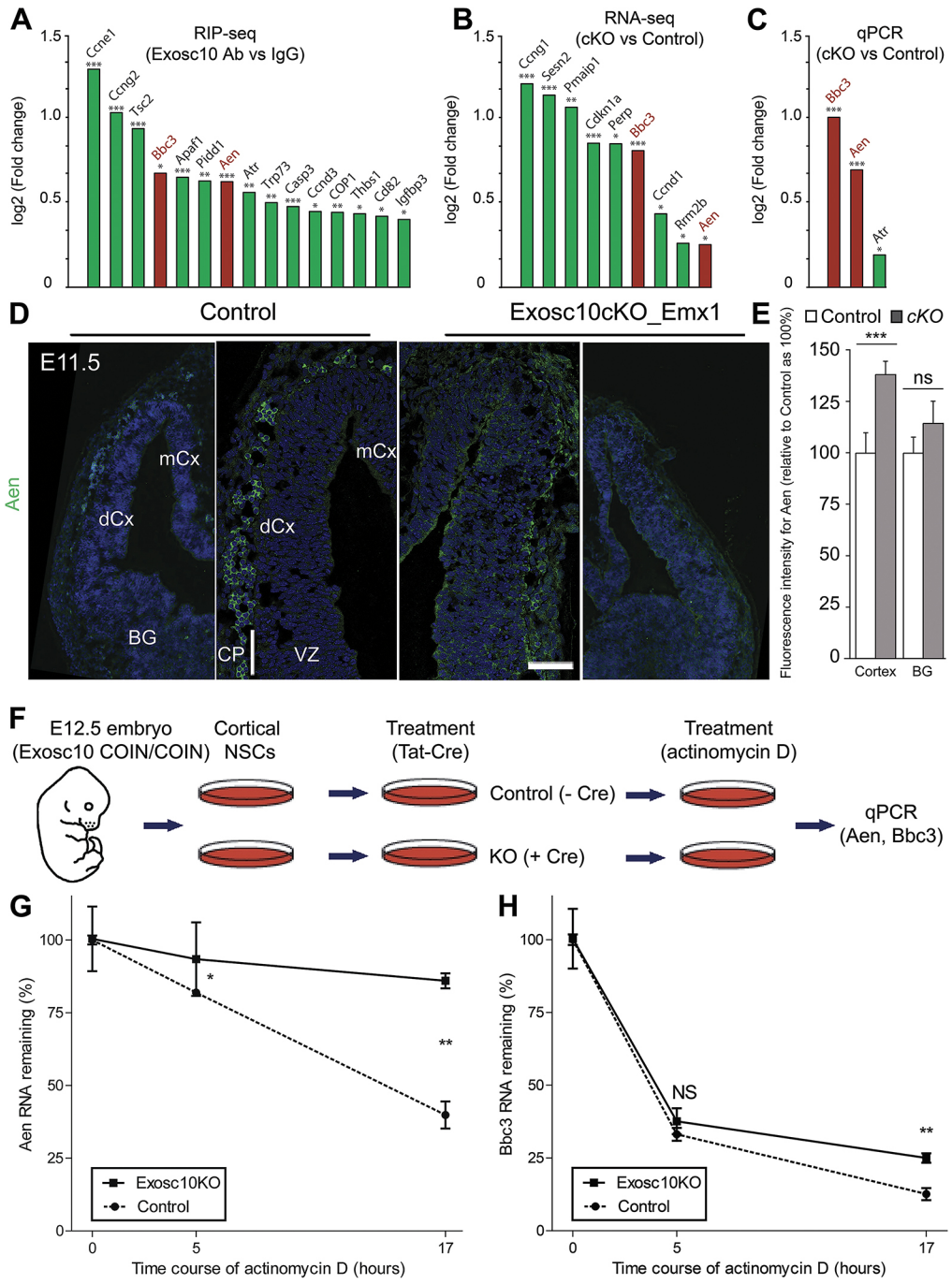

Fig. 6. Exosc10 suppresses the expression of P53 pathway *Aen* and *Bbc3* genes by degrading their transcripts. (A) RIP-seq analysis with RNA from E12.5 mouse cortex revealed the binding of Exosc10 to P53 pathway transcripts. (B,C) The upregulated genes in Exosc10cKO_Emx1-Cre cortex at E12.5, which are involved in P53 signaling, were identified by RNA-seq (B) and confirmed by qPCR (C). (D,E) Immunohistochemistry (D) and quantitative analyses (E) for expression of Aen on coronal sections of control and Exosc10cKO cortices at E11.5 are shown. (F) Experimental paradigm for the RNA degradation assay using cultured cortical NSCs. (G,H) RNA degradation assay showing changes in the RNA abundance of Aen (G) and Bbc3 (H) measured by qPCR from Exosc10 KO NSCs and control NSCs after actinomycin D treatment for 0 h, 5 h and 17 h. BG, basal ganglia; CP, cortical plate; dCx and mCx, dorsal and medial cortex; VZ, ventricular zone. **P*<0.05, ***P*<0.01, ****P*<0.005; NS, not significant. Scale bar: 100 µm.

concurrent reduction in the number of $Tbr2^{+}$ BPs leading to a thinner cortical plate in Ythdf2 KO embryos (Li et al., 2018). It should be noted, however, that m6A was shown to impact not only RNA stability but also other features of RNA metabolic processes, such as translation, splicing and transport of RNA (Dominissini et al., 2012; Meyer et al., 2012; Wang et al., 2014, 2015; Xiao et al., 2016). Thus, the precise roles of RNA stability in brain development are still largely unknown.

Functional investigations of genes encoding exosome subunits in model systems indicated that most exosome subunits are required for viability from yeast to man (Januszyk and Lima, 2014; Kilchert et al., 2016; Morton et al., 2018; Fasken et al., 2020). Although the precise role of the exosome complex in neural development is not known, mutations in four out of the 11 exosome subunit genes in humans have been found to be associated with neurodevelopmental and psychiatric disorders. Notably, mutations in Exosc2 are associated with intellectual disability (Di Donato et al., 2016), whereas mutations in Exosc3 (Wan et al., 2012; Rudnik-Schoneborn et al., 2013; Zanni et al., 2013; Eggens et al., 2014; Halevy et al., 2014), Exosc8 (Boczonadi et al., 2014) and Exosc9 (Burns et al., 2018) cause different types of cerebellar hypoplasia that lead to severe neurodegeneration and lethality. Mutations of these exosome factors were also associated with other brain defects, such as corpus callosum hypoplasia, cerebellar atrophy and abnormal myelination, as well as pontocerebellar hypoplasia with cerebellar and spinal motor neuron degeneration (Wan et al., 2012; Rudnik-Schoneborn et al., 2013; Zanni et al., 2013; Boczonadi et al., 2014; Eggens et al., 2014; Halevy et al., 2014; Di Donato

Development (2021) 148, dev188276. doi:10.1242/dev.188276

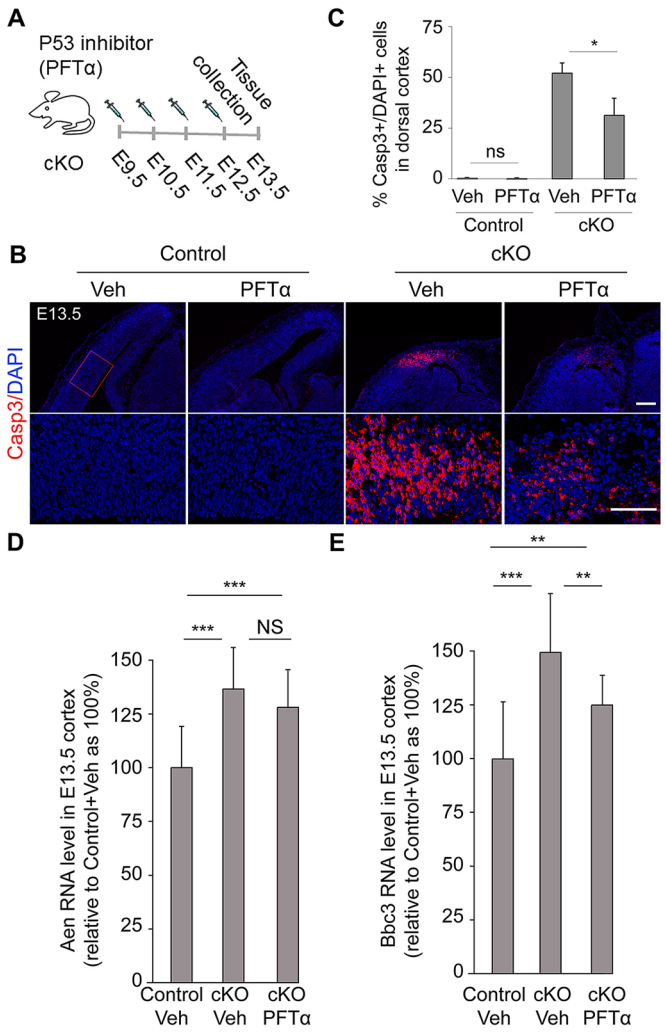

Fig. 7. Exosc10 suppresses apoptosis by inhibiting activity of P53 signaling pathway. (A) Rescue experimental paradigm with the P53 inhibitor (PFTα). (B,C) Immunohistochemistry (B) and quantitative analyses (C) for the apoptosis marker Casp3 on coronal sections of E13.5 control and Exosc10cKO cortices with or without PFTα treatment. Lower images are higher magnifications of field indicated by the red frame (B). The ratio of $Casp3^+$ cells to all $DAPI^+$ cells was assessed in control and Exosc10cKO cortices with or without PFTα treatment, showing a reduction in $Casp3^+$ cells in the cKO upon injection (C). (D,E) Treatment with PFTα decreases the expression of Bbc3 (E), but not that of Aen (D), which is upregulated in cKO cortex. *P<0.05, **P<0.01, ***P<0.005; NS, not significant. Scale bars: 200 µm and 100 µm (higher magnification.

et al., 2016; Burns et al., 2018). The findings in these human genetics studies indicate that the RNA exosome is crucial for normal neural development and cognition (Morton et al., 2018; Fasken et al., 2020).

Among Exosc subunits, the role of Exosc10 in biological processes is the most investigated. Exosc10 has been shown to stimulate mRNA turnover (Van Dijk et al., 2007), 3′ pre-rRNA processing (Knight et al., 2016), and decay of long non-coding and enhancer RNAs (eRNAs and lncRNAs) (Pefanis et al., 2015) with its absence causing RNA processing defects in yeast (Carneiro et al., 2007) and increased vulnerability to DNA damage (Rolfsmeier et al., 2011; Marin-Vicente et al., 2015; Domingo-Prim et al., 2019). Exosc10 functions with a co-factor, such as the NEXT complex, that recognizes and degrades RNA in DNA/RNA hybrid or RNA/RNA hybrid configuration, or eRNAs/lncRNAs (Lubas et al., 2011; Lim et al., 2017; Puno and Lima, 2018; Schmid and Jensen, 2019). Studies in cultured cell lines and in transgenic mice show that human Exosc10 is crucial for cell cycle (Blomen et al., 2015). More recent *in vivo* work reported that Exosc10 controls the onset of spermatogenesis in male germ cells (Jamin et al., 2017). Accordingly, Exosc10cKO mutant mice show small testes and impaired differentiation of germ cells, and exhibit reduced fertility (Jamin et al., 2017). However, whether or not Exosc10 is essential for brain development has remained unclear. Our findings reveal that the function of Exosc10 is required for the development of the forebrain. During early corticogenesis, Exosc10 is indispensable for cell viability and cortical layer formation. The requirement of the exosome complex in cell survival identified using the Exosc10cKO_*Emx1*-Cre cortex could possibly explain the aforementioned neurodegeneration caused by mutations of human Exosc genes.

The ring-like structured exosome complex contains eleven evolutionarily conserved subunits, including nine structural subunits (Exosc1-9) and two catalytic subunits (Exosc10 and Dis3) (Januszyk and Lima, 2014; Kilchert et al., 2016). The expression pattern analysis (Fig. S1B-J) revealed that many exosome subunits (e.g. Exosc1, Exosc2, Exosc3, Exosc5, Exosc9 and Exosc10) are widely expressed in developing mouse cortex. Remarkably, expression of some subunits is found to be limited to the VZ (Exosc8) or SVZ (Exosc7). This raises the question of whether all the components are required for the RNA exonuclease activity of the exosome complex. Even though our understanding of the functions of the exosome complex and its subunits in development has improved, several key questions remain unanswered. For example, is the composition of the exosome complex restricted to eleven subunits? Also, what is the contribution of individual subunits in formation and action of the exosome complex? Whether lineage-restricted subunits exist that lead to dynamic combinatorial assembly of exosome complexes, producing their biological specificity, remains to be determined. Efforts to resolve these and other questions would stimulate continuous interest in this area of research.

P53 pathway genes *Aen* and *Bbc3* are targets of Exosc10 in developing cortex

P53 is a well-known master regulator of numerous developmental events. It triggers expression of various downstream genes, some of which promote growth arrest and DNA repair, whereas others are involved in apoptosis (Mendrysa et al., 2011; Jain and Barton, 2018). The massive apoptosis observed in the early developing cortex of Exosc10cKO_*Emx1*-Cre embryos culminated in a severe reduction of cortical size.

To gain a transcriptome-wide insight into the role of exosome complex in corticogenesis, we carried out RNA-seq analysis of cKO cortices and Exosc10 RIP-seq. Our findings revealed upregulation of several genes associated with the P53 apoptosis pathway. Interestingly, cardinal components of apoptosis-associated P53 signaling, Aen (Kawase et al., 2008) and Bbc3 (Han et al., 2001; Jeffers et al., 2003), were identified in our RNA-seq and RIP-seq analyses. The RNA degradation assay carried out further highlighted that Exosc10 directly degrades transcripts of Aen and Bbc3.

Aen possesses exonuclease activity to degrade both DNA and RNA (Lee et al., 2005). In P53 signaling-dependent apoptosis, DNA damage signals lead to translocation of Aen into the nucleolus, causing nucleolar disruption (Kawase et al., 2008). Subsequently, Aen degrades DNA and RNA, amplifying the damage signal and inducing apoptosis (Kawase et al., 2008). The

Development (2021) 148, dev188276. doi:10.1242/dev.188276

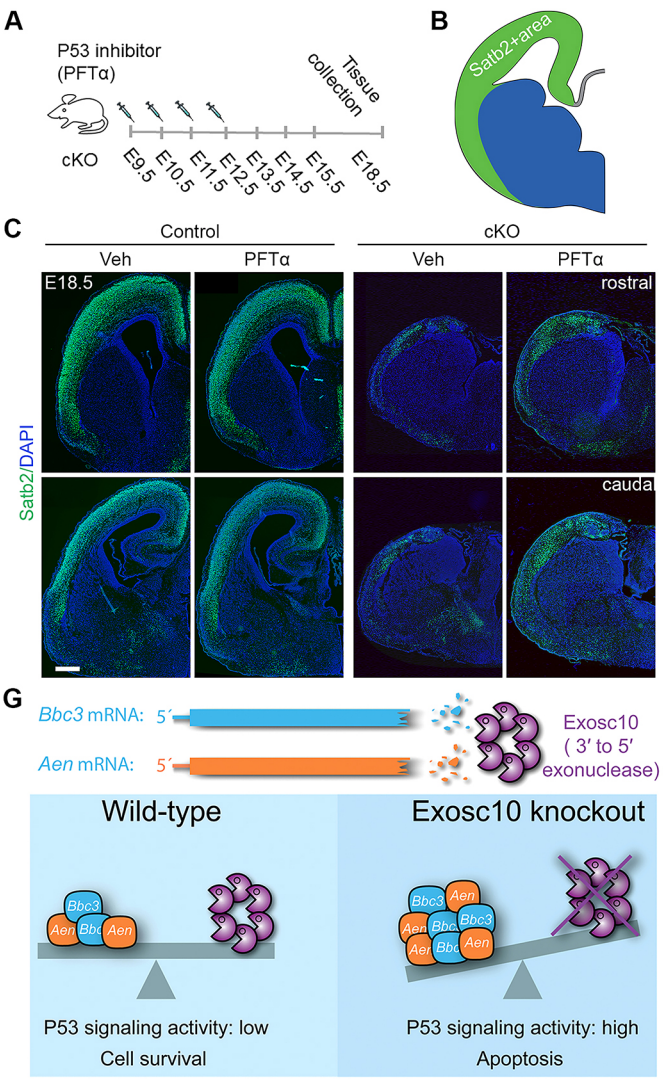

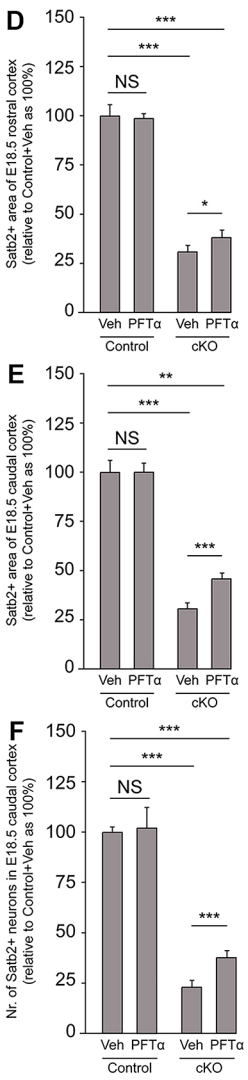

Fig. 8. Exosc10 controls cortical development partly by suppressing P53 signaling activity. (A,B) Rescue experimental paradigm (A) to examine effect of P53 signaling inhibitor (PFTα) on the Satb2$^+$ cortical area (B). (C-F) Immunohistochemistry with Satb2 antibody (C) and quantitative analyses (D-F) of cKO mutants at E18.5, showing the effects of treatment with PFTα on the Satb2$^+$ cortical area at rostral (D) and caudal (E) levels, and on the pool of Satb2$^+$ projection neurons at the caudal level (F). (G) A proposed model showing how the balanced level of RNA exonuclease Exosc10 and the P53 signaling factors Aen and Bbc3 ensures cell survival, whereas the loss of Exosc10 causes accumulation of Aen and Bbc3, leading to apoptosis. *P<0.05, **P<0.01, and ***P<0.005; NS, not significant. Scale bar: 200 µm.

promoter region of Bbc3 contains P53-binding sites and can be directly activated by P53 (Han et al., 2001). Bbc3 is part of the BH3-only BCL-2 family proteins, which have been found to localize to mitochondria in response to apoptotic stimuli, where they induce mitochondrial apoptosis (Huang and Strasser, 2000; Lomonosova and Chinnadurai, 2008). Bbc3 has been shown to be required for γ-irradiation-induced cell death in the developing brain, and P53 is not able to induce apoptosis in the absence of Bbc3 (Jeffers et al., 2003). Our data also highlight that Exosc10 regulates cell viability in developing cortex by repressing the distinct P53-dependent apoptosis signaling pathways, including those caused by DNA/RNA damage and γ-irradiation signals. Notably, PFTα treatment significantly rescues the aberrant upregulation of Bbc3 (but not Aen) upon the loss of Exosc10 in the developing cortex (Fig. 7D,E). This proves that Bbc3 (but not Aen) is a direct target of P53.

Previous studies indicated that accumulation of RNA/DNA hybrids or noncoding RNAs as eRNAs/lncRNAs could induce cellular genomic instability leading to P53 activation and cell death (Pefanis et al., 2015; Wolin and Maquat, 2019). In addition, RNA exosome is important for DNA DSB repair as the lack of Exosc10 leads to accumulation of DNA breaks and P53 activation (Pefanis et al., 2015; Domingo-Prim et al., 2019). The findings suggest that other mechanisms in addition to the increased expression of Aen and Bbc3 cause the hyperactivation of P53 signaling in response to the defect of RNA exosome activity.

In addition to the apoptotic P53 signaling pathway, we examined the oxidative stress signaling – one of the well-known cell death-triggering pathways in the developing brain (Green, 1998; Ikonomidou, 2009). Expression of genes encoding the main components of this pathway (e.g. BAX, BH3 and Cytochrome C) was unchanged in our RNA-seq analysis, and the pathway itself was not found in a corresponding GO study (Tables S1 and S2). Thus, our findings suggest that Exosc10 inhibits apoptosis mainly by suppressing the activity of the apoptotic P53 signaling pathway.

Pharmacological inhibition of P53 signaling rescued the described defects in cell viability in the Exosc10cKO mutants (Fig. 7A-C), suggesting that the Exosc complex negatively regulates P53 signaling during early cortical development. It is worth noting, however, that the inhibition of P53 signaling was not able to restore the normal thickness of cortical layers in Exosc10cKO mutants (Fig. 7A-C). Therefore, the observed drastic reduction in the size of the cortical plate cannot be singularly ascribed to the increased apoptosis but other unreported perturbations may contribute to the observed defective neurogenesis. In agreement with this assertion, our RNA-seq and RIP-seq data suggest that Exosc10 might directly suppress expression of many neuronal differentiation-associated genes. Possible defects in neurogenesis and neuronal differentiation

Development (2021) 148, dev188276. doi:10.1242/dev.188276

in the cortex-specific Exosc10cKO mutants will be in focus in a separate study.

Overall, our findings indicate a crucial role for Exosc10 in P53 pathway-mediated apoptosis, in which the binding of Exosc10 to the mRNAs of the P53 signaling mediators Aen and Bbc3 confers their rapid turnover. Our study indicates that suppression of P53 signaling by the exosome complex is essential for normal cell survival and brain development (Fig. 8G).

MATERIALS AND METHODS

Transgenic mice

Conditional inversion (COIN) alleles for Exosc10 (COIN/COIN) (Economides et al., 2013; Pefanis et al., 2015), *FoxG1-Cre* (Hébert and McConnell, 2000) and *Emx1-Cre* (Gorski et al., 2002) mice (*Mus musculus*) were maintained in a C57BL6/J background. Animals were handled in accordance with the German Animal Protection Law.

Antibodies

A list of antibodies is provided in the supplementary Materials and Methods.

Immunohistochemistry, western blotting and qPCR

Detailed descriptions have been provided previously (Narayanan et al., 2015) and more detail can be found in the supplementary Materials and Methods.

RNA-sequencing (RNA-seq), RNA-immunoprecipitation sequencing (RIP-seq) and bioinformatics analyses

Detailed descriptions have been provided previously for RNA-seq (Narayanan et al., 2015; Nguyen et al., 2018), RIP-seq (Yoon et al., 2017; Xie et al., 2019) and bioinformatics analyses (Narayanan et al., 2015; Nguyen et al., 2018). In RNA-seq experiments, RNA was obtained from cortex from five control and five Exosc10cKO embryos at E12.5. cDNA libraries were prepared using the TruSeq RNA Sample Preparation v2 Kit. DNA was quantified using a Nanodrop spectrophotometer, and its quality was assessed using an Agilent 2100 Bioanalyzer.

Exosc10 RNA-seq was performed using Magna RIP Kit (Merck Millipore) according to the manufacturer's instructions. In brief, dissociated cells from E12.5 cortex on 10 cm dish were lysed in 400 µl of complete RIP lysis buffer-containing protease inhibitors and RNase inhibitor. Exosc10 protein was pulled down using a Dynabeads-associated Exosc10 antibody. A mock pull-down was carried out with normal rabbit IgG (Cell Signaling Technologies). The immunoprecipitated complex was washed intensively and the pulled down RNA was extracted using Trizol reagent. Purified RNA was sequenced at the Transcriptome and Genome Analysis Laboratory (TAL) (University of Goettingen, Germany).

Data obtained from RNA- and RIP-seq were processed with the help of the Galaxy web platform (Afgan et al., 2018) and further analyzed using Webgestalt (http://www.webgestalt.org) (Wang et al., 2013, 2017; Zhang et al., 2005) and DAVID Bioinformatics Resources 6.8 (Huang et al., 2009). Gen sets from RNA- and RIP-seq were compared using Venny 2.1 (Oliveros). Base calling, fastq conversion, quality control and read alignments were all achieved as outlined for RIP-Seq. Reads were aligned to mouse genome mm10 and counted using FeaturesCount (http://bioinf.wehi.edu.au/featureCounts/). Differential expression was assessed using DESeq2 from Bioconductor (Love et al., 2014). Functional GO enrichment analyses were performed using ToppGene (Chen et al., 2009).

Culture and generation of Exosc10 KO primary NSCs

Mouse NSCs were isolated from E12.5 Exosc10 COIN/COIN cortices and cultured in NSC culture medium containing KO DMEM/F12 (Invitrogen), StemPro Neural Supplement (Invitrogen), Glutamax (Invitrogen), penicillin/streptomycin (Invitrogen), 20 ng/ml FGF2 (Invitrogen) and 20 ng/ml EGF (Invitrogen) on culture dishes precoated with 0.1% gelatin as described previously (Tuoc and Stoykova, 2008; Tuoc et al., 2013). TAT-Cre recombinase (Excellgen) (1 µM) was added to fresh NSC culture medium for 26 h to achieve Exosc10 KO.

RNA degradation assay

The assay was performed as described previously (Yoon et al., 2017; Xie et al., 2019). Briefly, Exosc10 COIN/COIN mouse NSCs were cultured to about 70-90% confluence. Some wells were treated with 1 µM TAT-Cre (Excellgen) 26 h beforehand to achieve Exosc10 KO; cells with vehicle solution served as controls. Actinomycin D (5 mM, Sigma) was supplemented to fresh NSC culture medium. Subsequently, cells were harvested at different time points (0 h, 5 h and 17 h) by washing once with PBS and detaching using Tripsin/EDTA (Sigma). For transcript quantification, RNA was extracted from the NSC samples. qPCR was carried out to quantify the transcript level of target genes. The experiment was performed in triplicate and normalized to internal 18S. Fold changes of transcript targets between Exosc10 KO and control NSCs were compared at different time points (0 h, 5 h and 17 h) after actinomycin D treatment. Fold changes at 5 h and 17 h were normalized to those at 0 h (before actinomycin D treatment).

In vivo pharmacological treatment and rescue experiments

Exosc10cKO_Emx1-Cre mouse embryos were subjected to the p53-inhibitor Pifithrin-α (PFT-α) (Komarov et al., 1999) by intraperitoneal injection of 2.2 mg/kg PFT-α (Selleckchem) into the pregnant mother at between E9.5 and E12.5 or between E9.5 and E15.5. Embryonic brains were isolated at E13.5 or E18.5 and immunohistochemistry was performed.

Relative quantification of cortical size

Dorsal views of forebrains of mutant and control mice were photographed under a dissection microscope. Cortical anterior-posterior axis (AP), cortical surface and midline lengths from the digitized images were measured with Fiji software to make comparison between mutants and controls. For further details, see the supplementary Materials and Methods.

Cell counts and quantitative analysis of IHC signal intensity

IHC quantification was performed using anatomically matched coronal sections. In most cases, cell counts of six matched sections were averaged (control/cKO). For quantitative analyses of IHC signal intensity of cytoplasm-staining markers, fluorescent images of selected areas of the cortex were used. Color images were converted to gray scale and the fluorescent signal intensity values were measured using the Analyze/Measure function of Fiji software. The signal intensity from the background next to the tissue was subtracted from the measured intensity for normalization. For further details, see the supplementary Materials and Methods.

Image acquisition and statistical analysis

Imaging was performed with an Axio Imager M2 (Zeiss) with a Neurolucida system (Version 11; MBF Bioscience) and a confocal fluorescence microscope (TCS SP5; Leica). Images were further analyzed with Adobe Photoshop and Fiji. Statistical analyses were carried out using Student's *t*-test. Graphs are plotted as mean±s.e.m. An unpaired *t*-test was carried out on the average from at least three biological replicates. All details of statistical analyses and description for histological experiments are presented in Table S7 and in the supplementary Materials and Methods.

Acknowledgements

We acknowledge T. Huttanus and M. Blessmann for their expert animal care and support. We also thank F. Guillemot, A. Nave, A. P. McMahon, A. Jones and O. Machon for providing reagents.

Competing interests

The authors declare no competing or financial interests.

Author contributions

Conceptualization: T.T.; Methodology: Y.X., O.S., T.T.; Validation: T.T.; Formal analysis: P.A.U., G.S., L.P., O.S., J.R., T.B., A.F.; Investigation: P.A.U., Y.X., L.P., T.B., A.F.; Resources: U.B., H.P.N., J.F.S., T.T.; Writing - original draft: P.A.U.; Writing - review & editing: G.S., T.T.; Supervision: T.T.; Project administration: T.T.; Funding acquisition: H.P.N., J.F.S., T.T.

Funding

This work was supported by the Deutsche Forschungsgemeinschaft (TU432/1-1, TU432/3-1 and TU432/6-1 to T.T.), by the Schram-Stiftung (T.T.) and by the National

Institutes of Health/National Institute of Allergy and Infectious Diseases (AI134988 to U.B.). Deposited in PMC for release after 12 months.

Data availability

All RNA-Seq and RIP-Seq data have been deposited in GEO under accession number GSE164188.

Supplementary information

Supplementary information available online at
https://dev.biologists.org/lookup/doi/10.1242/dev.188276.supplemental

Peer review history

The peer review history is available online at
https://dev.biologists.org/lookup/doi/10.1242/dev.188276.reviewer-comments.pdf

References

Afgan, E., Baker, D., Batut, B., van den Beek, M., Bouvier, D., Čech, M., Chilton, J., Clements, D., Coraor, N., Gruning, B. A. et al. (2018). The Galaxy platform for accessible, reproducible and collaborative biomedical analyses: 2018 update. *Nucleic Acids Res.* **46**, W537-W544. doi:10.1093/nar/gky379

Alcamo, E. A., Chirivella, L., Dautzenberg, M., Dobreva, G., Fariñas, I., Grosschedl, R. and McConnell, S. K. (2008). Satb2 regulates callosal projection neuron identity in the developing cerebral cortex. *Neuron* **57**, 364-377. doi:10.1016/j.neuron.2007.12.012

Blomen, V. A., Majek, P., Jae, L. T., Bigenzahn, J. W., Nieuwenhuis, J., Staring, J., Sacco, R., van Diemen, F. R., Olk, N., Stukalov, A. et al. (2015). Gene essentiality and synthetic lethality in haploid human cells. *Science* **350**, 1092-1096. doi:10.1126/science.aac7557

Boczonadi, V., Müller, J. S., Pyle, A., Munkley, J., Dor, T., Quartararo, J., Ferrero, I., Karcagi, V., Giunta, M., Polvikoski, T. et al. (2014). EXOSC8 mutations alter mRNA metabolism and cause hypomyelination with spinal muscular atrophy and cerebellar hypoplasia. *Nat. Commun.* **5**, 4287. doi:10.1038/ncomms5287

Britanova, O., de Juan Romero, C., Cheung, A., Kwan, K. Y., Schwark, M., Gyorgy, A., Vogel, T., Akopov, S., Mitkovski, M., Agoston, D. et al. (2008). Satb2 is a postmitotic determinant for upper-layer neuron specification in the neocortex. *Neuron* **57**, 378-392. doi:10.1016/j.neuron.2007.12.028

Burns, D. T., Donkervoort, S., Müller, J. S., Knierim, E., Bharucha-Goebel, D., Faqeih, E. A., Bell, S. K., AlFaifi, A. Y., Monies, D., Millan, F. et al. (2018). Variants in EXOSC9 disrupt the RNA exosome and result in cerebellar atrophy with spinal motor neuronopathy. *Am. J. Hum. Genet.* **102**, 858-873. doi:10.1016/j.ajhg.2018.03.011

Carneiro, T., Carvalho, C., Braga, J., Rino, J., Milligan, L., Tollervey, D. and Carmo-Fonseca, M. (2007). Depletion of the yeast nuclear exosome subunit Rrp6 results in accumulation of polyadenylated RNAs in a discrete domain within the nucleolus. *Mol. Cell. Biol.* **27**, 4157-4165. doi:10.1128/MCB.00120-07

Chen, J., Bardes, E. E., Aronow, B. J. and Jegga, A. G. (2009). ToppGene suite for gene list enrichment analysis and candidate gene prioritization. *Nucleic Acids Res.* **37**, W305-W311. doi:10.1093/nar/gkp427

Di Donato, N., Neuhann, T., Kahlert, A.-K., Klink, B., Hackmann, K., Neuhann, I., Novotna, B., Schallner, J., Krause, C., Glass, I. A. et al. (2016). Mutations in EXOSC2 are associated with a novel syndrome characterised by retinitis pigmentosa, progressive hearing loss, premature ageing, short stature, mild intellectual disability and distinctive gestalt. *J. Med. Genet.* **53**, 419-425. doi:10.1136/jmedgenet-2015-103511

Domingo-Prim, J., Endara-Coll, M., Bonath, F., Jimeno, S., Prados-Carvaja, R., Friedländer, M. R., Huertas, P. and Visa, N. (2019). EXOSC10 is required for RPA assembly and controlled DNA end resection at DNA double-strand breaks. *Nat. Commun.* **10**, 2135. doi:10.1038/s41467-019-10153-9

Dominissini, D., Moshitch-Moshkovitz, S., Schwartz, S., Salmon-Divon, M., Ungar, L., Osenberg, S., Cesarkas, K., Jacob-Hirsch, J., Amariglio, N., Kupiec, M. et al. (2012). Topology of the human and mouse m6A RNA methylomes revealed by m6A-seq. *Nature* **485**, 201-206. doi:10.1038/nature11112

Economides, A. N., Frendewey, D., Yang, P., Dominguez, M. G., Dore, A. T., Lobov, I. B., Persaud, T., Rojas, J., McClain, J., Lengyel, P. et al. (2013). Conditionals by inversion provide a universal method for the generation of conditional alleles. *Proc. Natl. Acad. Sci. USA* **110**, E3179-E3188. doi:10.1073/pnas.1217812110

Eggens, V. R. C., Barth, P. G., Niermeijer, J.-M. F., Berg, J. N., Darin, N., Dixit, A., Fluss, J., Foulds, N., Fowler, D., Hortobágyi, T. et al. (2014). EXOSC3 mutations in pontocerebellar hypoplasia type 1: novel mutations and genotype-phenotype correlations. *Orphanet J. Rare Dis.* **9**, 23. doi:10.1186/1750-1172-9-23

Fasken, M. B., Morton, D. J., Kuiper, E. G., Jones, S. K., Leung, S. W. and Corbett, A. H. (2020). The RNA exosome and human disease. *Methods Mol. Biol.* **2062**, 3-33. doi:10.1007/978-1-4939-9822-7_1

Flamand, M. N. and Meyer, K. D. (2019). The epitranscriptome and synaptic plasticity. *Curr. Opin. Neurobiol.* **59**, 41-48. doi:10.1016/j.conb.2019.04.007

Gorski, J. A., Talley, T., Qiu, M., Puelles, L., Rubenstein, J. L. R. and Jones, K. R. (2002). Cortical excitatory neurons and glia, but not GABAergic neurons, are produced in the Emx1-expressing lineage. *J. Neurosci.* **22**, 6309-6314. doi:10.1523/JNEUROSCI.22-15-06309.2002

Götz, M. and Huttner, W. B. (2005). The cell biology of neurogenesis. *Nat. Rev. Mol. Cell Biol.* **6**, 777-788. doi:10.1038/nrm1739

Green, D. R. (1998). Apoptotic pathways: the roads to ruin. *Cell* **94**, 695-698. doi:10.1016/S0092-8674(00)81728-6

Halevy, A., Lerer, I., Cohen, R., Kornreich, L., Shuper, A., Gamliel, M., Zimerman, B.-E., Korabi, I., Meiner, V., Straussberg, R. et al. (2014). Novel EXOSC3 mutation causes complicated hereditary spastic paraplegia. *J. Neurol.* **261**, 2165-2169. doi:10.1007/s00415-014-7457-x

Han, J.-W., Flemington, C., Houghton, A. B., Gu, Z., Zambetti, G. P., Lutz, R. J., Zhu, L. and Chittenden, T. (2001). Expression of bbc3, a pro-apoptotic BH3-only gene, is regulated by diverse cell death and survival signals. *Proc. Natl. Acad. Sci. USA* **98**, 11318-11323. doi:10.1073/pnas.201208798

Hébert, J. M. and McConnell, S. K. (2000). Targeting of cre to the Foxg1 (BF-1) locus mediates loxP recombination in the telencephalon and other developing head structures. *Dev. Biol.* **222**, 296-306. doi:10.1006/dbio.2000.9732

Huang, D. C. S. and Strasser, A. (2000). BH3-only proteins—essential initiators of apoptotic cell death. *Cell* **103**, 839-842. doi:10.1016/S0092-8674(00)00187-2

Huang, D. W., Sherman, B. T. and Lempicki, R. A. (2009). Bioinformatics enrichment tools: paths toward the comprehensive functional analysis of large gene lists. *Nucleic Acids Res.* **37**, 1-13. doi:10.1093/nar/gkn923

Ikonomidou, C. (2009). Triggers of apoptosis in the immature brain. *Brain Dev.* **31**, 488-492. doi:10.1016/j.braindev.2009.02.006

Jain, A. K. and Barton, M. C. (2018). p53: emerging roles in stem cells, development and beyond. *Development* **145**, dev158360. doi:10.1242/dev.158360

Jamin, S. P., Petit, F. G., Kervarrec, C., Smagulova, F., Illner, D., Scherthan, H. and Primig, M. (2017). EXOSC10/Rrp6 is post-translationally regulated in male germ cells and controls the onset of spermatogenesis. *Sci. Rep.* **7**, 15065. doi:10.1038/s41598-017-14643-y

Januszyk, K. and Lima, C. D. (2014). The eukaryotic RNA exosome. *Curr. Opin. Struct. Biol.* **24**, 132-140. doi:10.1016/j.sbi.2014.01.011

Jeffers, J. R., Parganas, E., Lee, Y., Yang, C., Wang, J. L., Brennan, J., MacLean, K. H., Han, J., Chittenden, T., Ihle, J. N. et al. (2003). Puma is an essential mediator of p53-dependent and -independent apoptotic pathways. *Cancer Cell* **4**, 321-328. doi:10.1016/S1535-6108(03)00244-7

Kawase, T., Ichikawa, H., Ohta, T., Nozaki, N., Tashiro, F., Ohki, R. and Taya, Y. (2008). p53 target gene AEN is a nuclear exonuclease required for p53-dependent apoptosis. *Oncogene* **27**, 3797-3810. doi:10.1038/onc.2008.32

Kilchert, C., Wittmann, S. and Vasiljeva, L. (2016). The regulation and functions of the nuclear RNA exosome complex. *Nat. Rev. Mol. Cell Biol.* **17**, 227-239. doi:10.1038/nrm.2015.15

Knight, J. R. P., Bastide, A., Peretti, D., Roobol, A., Roobol, J., Mallucci, G. R., Smales, C. M. and Willis, A. E. (2016). Cooling-induced SUMOylation of EXOSC10 down-regulates ribosome biogenesis. *RNA* **22**, 623-635. doi:10.1261/rna.054411.115

Komarov, P. G., Komarova, E. A., Kondratov, R. V., Christov-Tselkov, K., Coon, J. S., Chernov, M. V. and Gudkov, A. V. (1999). A chemical inhibitor of p53 that protects mice from the side effects of cancer therapy. *Science* **285**, 1733-1737. doi:10.1126/science.285.5434.1733

Kriegstein, A., Noctor, S. and Martínez-Cerdeño, V. (2006). Patterns of neural stem and progenitor cell division may underlie evolutionary cortical expansion. *Nat. Rev. Neurosci.* **7**, 883-890. doi:10.1038/nrn2008

Lee, J.-H., Koh, Y. A., Cho, C.-K., Lee, S.-J., Lee, Y.-S. and Bae, S. (2005). Identification of a novel ionizing radiation-induced nuclease, AEN, and its functional characterization in apoptosis. *Biochem. Biophys. Res. Commun.* **337**, 39-47. doi:10.1016/j.bbrc.2005.08.264

Li, M., Zhao, X., Wang, W., Shi, H., Pan, Q., Lu, Z., Perez, S. P., Suganthan, R., He, C., Bjørås, M. et al. (2018). Ythdf2-mediated m^{6}A mRNA clearance modulates neural development in mice. *Genome Biol.* **19**, 69. doi:10.1186/s13059-018-1436-y

Lim, J., Giri, P. K., Kazadi, D., Laffleur, B., Zhang, W., Grinstein, V., Pefanis, E., Brown, L. M., Ladewig, E., Martin, O. et al. (2017). Nuclear proximity of Mtr4 to RNA exosome restricts DNA mutational asymmetry. *Cell* **169**, 523-537.e15. doi:10.1016/j.cell.2017.03.043

Liu, J., Yue, Y., Han, D., Wang, X., Fu, Y., Zhang, L., Jia, G., Yu, M., Lu, Z., Deng, X. et al. (2014). A METTL3-METTL14 complex mediates mammalian nuclear RNA N6-adenosine methylation. *Nat. Chem. Biol.* **10**, 93-95. doi:10.1038/nchembio.1432

Lomonosova, E. and Chinnadurai, G. (2008). BH3-only proteins in apoptosis and beyond: an overview. *Oncogene* **27** Suppl. 1, S2-S19. doi:10.1038/onc.2009.39

Love, M. I., Huber, W. and Anders, S. (2014). Moderated estimation of fold change and dispersion for RNA-seq data with DESeq2. *Genome Biol.* **15**, 550.

Lubas, M., Christensen, M. S., Kristiansen, M. S., Domanski, M., Falkenby, L. G., Lykke-Andersen, S., Andersen, J. S., Dziembowski, A. and Jensen, T. H. (2011). Interaction profiling identifies the human nuclear exosome targeting complex. *Mol. Cell* **43**, 624-637. doi:10.1016/j.molcel.2011.06.028

Marin-Vicente, C., Domingo-Prim, J., Eberle, A. B. and Visa, N. (2015). RRP6/EXOSC10 is required for the repair of DNA double-strand breaks by homologous recombination. *J. Cell Sci.* **128**, 1097-1107. doi:10.1242/jcs.158733

Mendrysa, S. M., Ghassemifar, S. and Malek, R. (2011). p53 in the CNS: perspectives on development, stem cells, and cancer. *Genes Cancer* **2**, 431-442. doi:10.1177/1947601911409736

Meyer, K. D., Saletore, Y., Zumbo, P., Elemento, O., Mason, C. E. and Jaffrey, S. R. (2012). Comprehensive analysis of mRNA methylation reveals enrichment in 3′ UTRs and near stop codons. *Cell* **149**, 1635-1646. doi:10.1016/j.cell.2012.05.003

Meyer, K. D., Patil, D. P., Zhou, J., Zinoviev, A., Skabkin, M. A., Elemento, O., Pestova, T. V., Qian, S.-B. and Jaffrey, S. R. (2015). 5′ UTR m^6A promotes cap-independent translation. *Cell* **163**, 999-1010. doi:10.1016/j.cell.2015.10.012

Morton, D. J., Kuiper, E. G., Jones, S. K., Leung, S. W., Corbett, A. H. and Fasken, M. B. (2018). The RNA exosome and RNA exosome-linked disease. *RNA* **24**, 127-142. doi:10.1261/rna.064626.117

Narayanan, R., Pirouz, M., Kerimoglu, C., Pham, L., Wagener, R. J., Kiszka, K. A., Rosenbusch, J., Seong, R. H., Kessel, M., Fischer, A. et al. (2015). Loss of BAF (mSWI/SNF) complexes causes global transcriptional and chromatin state changes in forebrain development. *Cell Rep.* **13**, 1842-1854. doi:10.1016/j.celrep.2015.10.046

Nguyen, H., Kerimoglu, C., Pirouz, M., Pham, L., Kiszka, K. A., Sokpor, G., Sakib, M. S., Rosenbusch, J., Teichmann, U., Seong, R. H. et al. (2018). Epigenetic regulation by BAF complexes limits neural stem cell proliferation by suppressing Wnt signaling in late embryonic development. *Stem Cell Rep.* **10**, 1734-1750. doi:10.1016/j.stemcr.2018.04.014

Patil, D. P., Chen, C.-K., Pickering, B. F., Chow, A., Jackson, C., Guttman, M. and Jaffrey, S. R. (2016). m^6A RNA methylation promotes XIST-mediated transcriptional repression. *Nature* **537**, 369-373. doi:10.1038/nature19342

Pefanis, E., Wang, J., Rothschild, G., Lim, J., Kazadi, D., Sun, J., Federation, A., Chao, J., Elliott, O., Liu, Z.-P. et al. (2015). RNA exosome-regulated long non-coding RNA transcription controls super-enhancer activity. *Cell* **161**, 774-789. doi:10.1016/j.cell.2015.04.034

Pontious, A., Kowalczyk, T., Englund, C. and Hevner, R. F. (2008). Role of intermediate progenitor cells in cerebral cortex development. *Dev. Neurosci.* **30**, 24-32. doi:10.1159/000109848

Puno, M. R. and Lima, C. D. (2018). Structural basis for MTR4-ZCCHC8 interactions that stimulate the MTR4 helicase in the nuclear exosome-targeting complex. *Proc. Natl. Acad. Sci. USA* **115**, E5506-E5515. doi:10.1073/pnas.1803530115

Rolfsmeier, M. L., Laughery, M. F. and Haseltine, C. A. (2011). Repair of DNA double-strand breaks induced by ionizing radiation damage correlates with upregulation of homologous recombination genes in Sulfolobus solfataricus. *J. Mol. Biol.* **414**, 485-498. doi:10.1016/j.jmb.2011.10.020

Rudnik-Schoneborn, S., Senderek, J., Jen, J. C., Houge, G., Seeman, P., Puchmajerova, A., Graul-Neumann, L., Seidel, U., Korinthenberg, R., Kirschner, J. et al. (2013). Pontocerebellar hypoplasia type 1: clinical spectrum and relevance of EXOSC3 mutations. *Neurology* **80**, 438-446. doi:10.1212/WNL.0b013e31827f0f66

Schmid, M. and Jensen, T. H. (2019). The nuclear RNA exosome and its cofactors. *Adv. Exp. Med. Biol.* **1203**, 113-132. doi:10.1007/978-3-030-31434-7_4

Telley, L., Govindan, S., Prados, J., Stevant, I., Nef, S., Dermitzakis, E., Dayer, A. and Jabaudon, D. (2016). Sequential transcriptional waves direct the differentiation of newborn neurons in the mouse neocortex. *Science* **351**, 1443-1446. doi:10.1126/science.aad8361

Tuoc, T. C. and Stoykova, A. (2008). Trim11 modulates the function of neurogenic transcription factor Pax6 through ubiquitin-proteosome system. *Genes Dev.* **22**, 1972-1986. doi:10.1101/gad.471708

Tuoc, T. C., Boretius, S., Sansom, S. N., Pitulescu, M.-E., Frahm, J., Livesey, F. J. and Stoykova, A. (2013). Chromatin regulation by BAF170 controls cerebral cortical size and thickness. *Dev. Cell* **25**, 256-269. doi:10.1016/j.devcel.2013.04.005

Van Dijk, E. L., Schilders, G. and Pruijn, G. J. M. (2007). Human cell growth requires a functional cytoplasmic exosome, which is involved in various mRNA decay pathways. *RNA* **13**, 1027-1035. doi:10.1261/rna.575107

Visel, A., Thaller, C. and Eichele, G. (2004). GenePaint.org: an atlas of gene expression patterns in the mouse embryo. *Nucleic Acids Res.* **32**, D552-D556. doi:10.1093/nar/gkh029

Wan, J., Yourshaw, M., Mamsa, H., Rudnik-Schöneborn, S., Menezes, M. P., Hong, J. E., Leong, D. W., Senderek, J., Salman, M. S., Chitayat, D. et al. (2012). Mutations in the RNA exosome component gene EXOSC3 cause pontocerebellar hypoplasia and spinal motor neuron degeneration. *Nat. Genet.* **44**, 704-708. doi:10.1038/ng.2254

Wang, J., Duncan, D., Shi, Z. and Zhang, B. (2013). WEB-based GEne SeT AnaLysis Toolkit (WebGestalt): update 2013. *Nucleic Acids Res.* **41**, W77-W83. doi:10.1093/nar/gkt439

Wang, X., Lu, Z., Gomez, A., Hon, G. C., Yue, Y., Han, D., Fu, Y., Parisien, M., Dai, Q., Jia, G. et al. (2014). N6-methyladenosine-dependent regulation of messenger RNA stability. *Nature* **505**, 117-120. doi:10.1038/nature12730

Wang, X., Zhao, B. S., Roundtree, I. A., Lu, Z., Han, D., Ma, H., Weng, X., Chen, K., Shi, H. and He, C. (2015). N^6-methyladenosine modulates messenger RNA translation efficiency. *Cell* **161**, 1388-1399. doi:10.1016/j.cell.2015.05.014

Wang, X., Feng, J., Xue, Y., Guan, Z., Zhang, D., Liu, Z., Gong, Z., Wang, Q., Huang, J., Tang, C. et al. (2016). Structural basis of N^6-adenosine methylation by the METTL3–METTL14 complex. *Nature* **534**, 575-578. doi:10.1038/nature18298

Wang, J., Vasaikar, S., Shi, Z., Greer, M. and Zhang, B. (2017). WebGestalt 2017: a more comprehensive, powerful, flexible and interactive gene set enrichment analysis toolkit. *Nucleic Acids Res.* **45**, W130-W137. doi:10.1093/nar/gkx356

Wang, Y., Li, Y., Yue, M., Wang, J., Kumar, S., Wechsler-Reya, R. J., Zhang, Z., Ogawa, Y., Kellis, M., Duester, G. et al. (2018). N^6-methyladenosine RNA modification regulates embryonic neural stem cell self-renewal through histone modifications. *Nat. Neurosci.* **21**, 195-206. doi:10.1038/s41593-017-0057-1

Widagdo, J. and Anggono, V. (2018). The m6A-epitranscriptomic signature in neurobiology: from neurodevelopment to brain plasticity. *J. Neurochem.* **147**, 137-152. doi:10.1111/jnc.14481

Wolin, S. L. and Maquat, L. E. (2019). Cellular RNA surveillance in health and disease. *Science* **366**, 822-827. doi:10.1126/science.aax2957

Xiao, W., Adhikari, S., Dahal, U., Chen, Y.-S., Hao, Y.-J., Sun, B.-F., Sun, H.-Y., Li, A., Ping, X.-L., Lai, W.-Y. et al. (2016). Nuclear m^6A reader YTHDC1 regulates mRNA splicing. *Mol. Cell* **61**, 507-519. doi:10.1016/j.molcel.2016.01.012

Xie, Y., Castro-Hernández, R., Sokpor, G., Pham, L., Narayanan, R., Rosenbusch, J., Staiger, J. F. and Tuoc, T. (2019). RBM15 modulates the function of chromatin remodeling factor BAF155 through RNA methylation in developing cortex. *Mol. Neurobiol.* **56**, 7305-7320. doi:10.1007/s12035-019-1595-1

Yoon, K.-J., Ringeling, F. R., Vissers, C., Jacob, F., Pokrass, M., Jimenez-Cyrus, D., Su, Y., Kim, N.-S., Zhu, Y., Zheng, L. et al. (2017). Temporal control of mammalian cortical neurogenesis by m^6A methylation. *Cell* **171**, 877-889.E17. doi:10.1016/j.cell.2017.09.003

Zanni, G., Scotton, C., Passarelli, C., Fang, M., Barresi, S., Dallapiccola, B., Wu, B., Gualandi, F., Ferlini, A., Bertini, E. et al. (2013). Exome sequencing in a family with intellectual disability, early onset spasticity, and cerebellar atrophy detects a novel mutation in EXOSC3. *Neurogenetics* **14**, 247-250. doi:10.1007/s10048-013-0371-z

Zhang, B., Kirov, S. and Snoddy, J. (2005). WebGestalt: an integrated system for exploring gene sets in various biological contexts. *Nucleic Acids Res.* **33**, W741-W748. doi:10.1093/nar/gki475

Zheng, G., Dahl, J. A., Niu, Y., Fedorcsak, P., Huang, C.-M., Li, C. J., Vågbø, C. B., Shi, Y., Wang, W.-L., Song, S.-H. et al. (2013). ALKBH5 is a mammalian RNA demethylase that impacts RNA metabolism and mouse fertility. *Mol. Cell* **49**, 18-29. doi:10.1016/j.molcel.2012.10.015

SUPPLEMENTAL DATA

Supplementary Figure 1

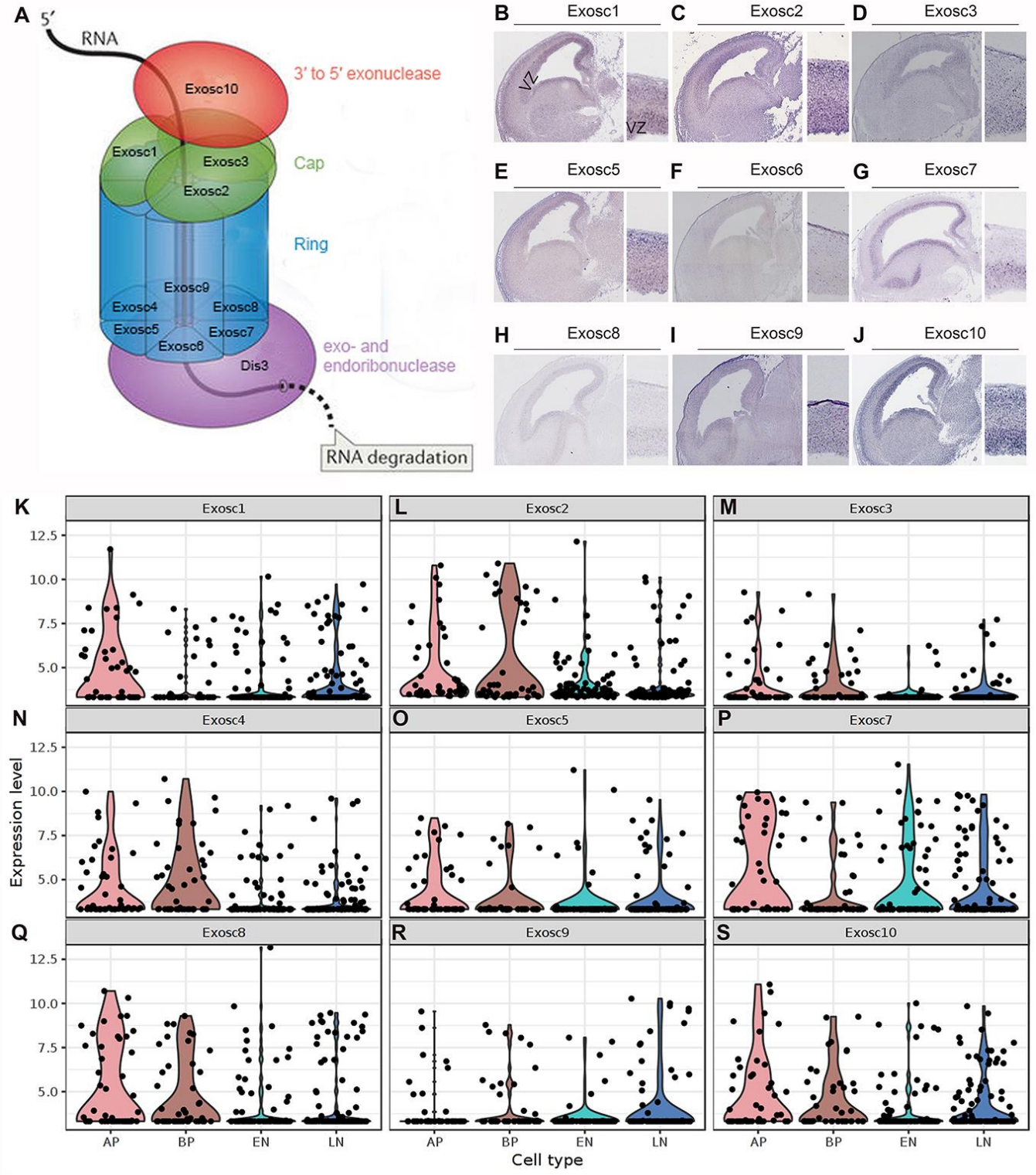

Figure S1. Expression of exosome complex subunits in the developing mouse brain.

(A) Model structure of the exosome complex with its components (Kilchert et al. 2016). (B–J) *In situ* hybridization of exosome complex components in sagittal sections of the E14.5 brains obtained from GenePaint database (Visel et al. 2004). Higher magnification of the cortex on right panels shows a high expression of exosome genes in the cortex, especially in the ventricular zone (VZ). (K–S) Expression of exosome subunits based on a published single-cell RNA-seq dataset of embryonic mouse cortex (Telley et al. 2016). The expression profiles of exosome subunits as violin plots was generated using the Seurat package of R (http://genebrowser.unige.ch/science2016/) (Macosko et al. 2015). AP: Apical progenitors/RGCs; BP: daughter basal progenitors/IPCs; EN: early-born neurons; LN: late-born neurons.

Supplementary Figure 2

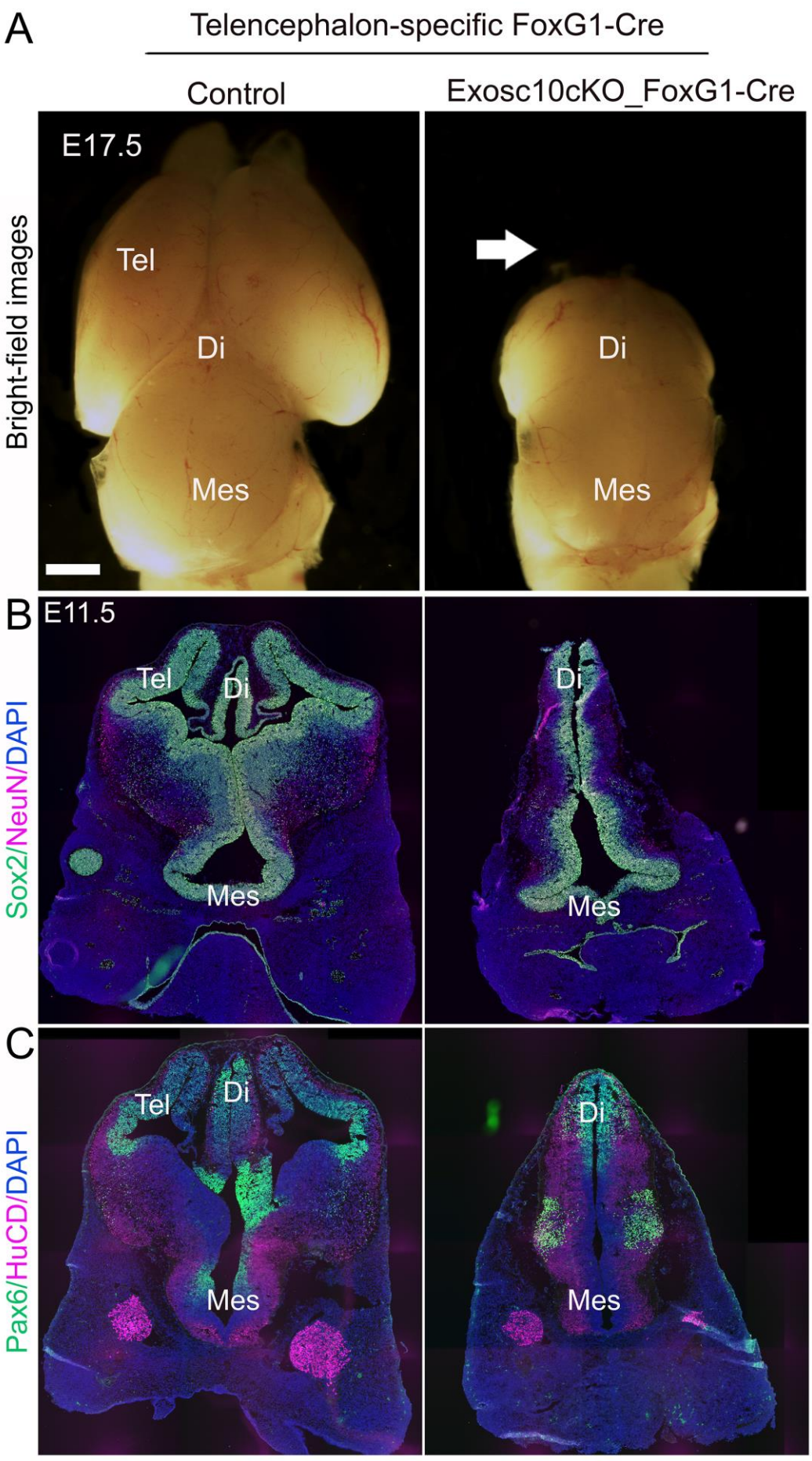

Figure S2. Expression of Exosc10 is required for specification of telencephalon.

(A) The forebrain-specific *dcKO_FoxG1*-Cre embryos have no telencephalon. (B, C) Representative images show IHC analyses with coronal sections of head from control and cKO_FoxG1-Cre embryos at E11.5 with antibodies against Sox2, NeuN (B) and Pax6, HuCD (C) that specifically label primordial NSC markers Sox2, Pax6, and immature neuronal markers NeuN, and HuCD respectively. IHC analyses revealed detectable Sox2+, Pax6+ NSCs and HuCD+, NeuN+ neurons in Diencephalon (Di) and in mesencephalon (Mes) in both control and cKO head, whereas these cell types were detected only in dorsolateral part (telencephalon, Tel) of control, but not that of cKO head. Abbreviations: Tel, telencephalon; Di, diencephalon; Mes, mesencephalon. Scale bars = 1 mm.

Supplementary Figure 3

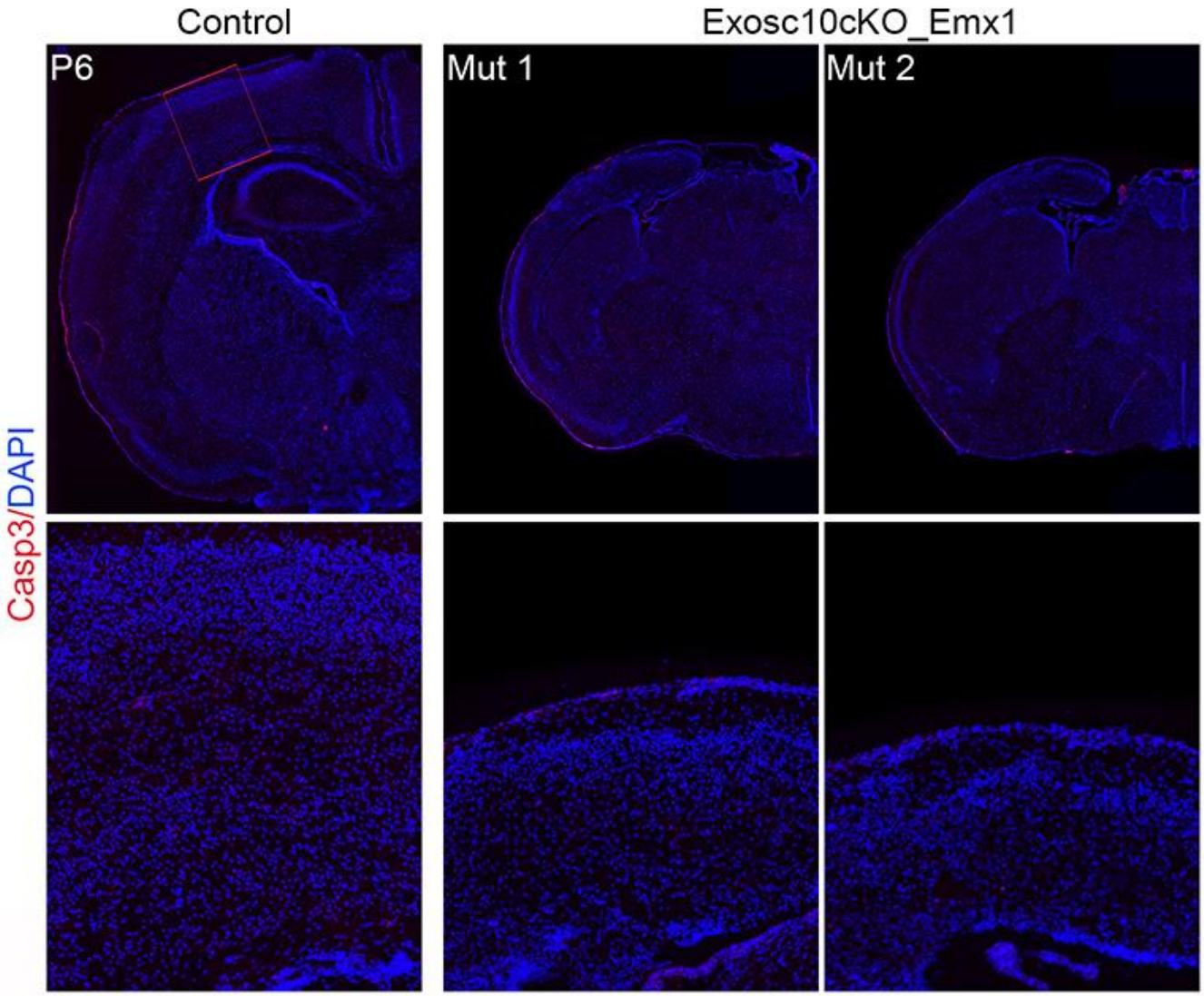

Figure S3. Exosc10 expression is not required for cell viability in postnatal cortex.

IHC analysis with antibody against Casp3 to detect cell death (counter staining with DAPI) indicated there was no obvious difference in number of Casp3+ apoptotic cells between control and Exosc10cKO cortices at P6.

Supplementary Figure 4

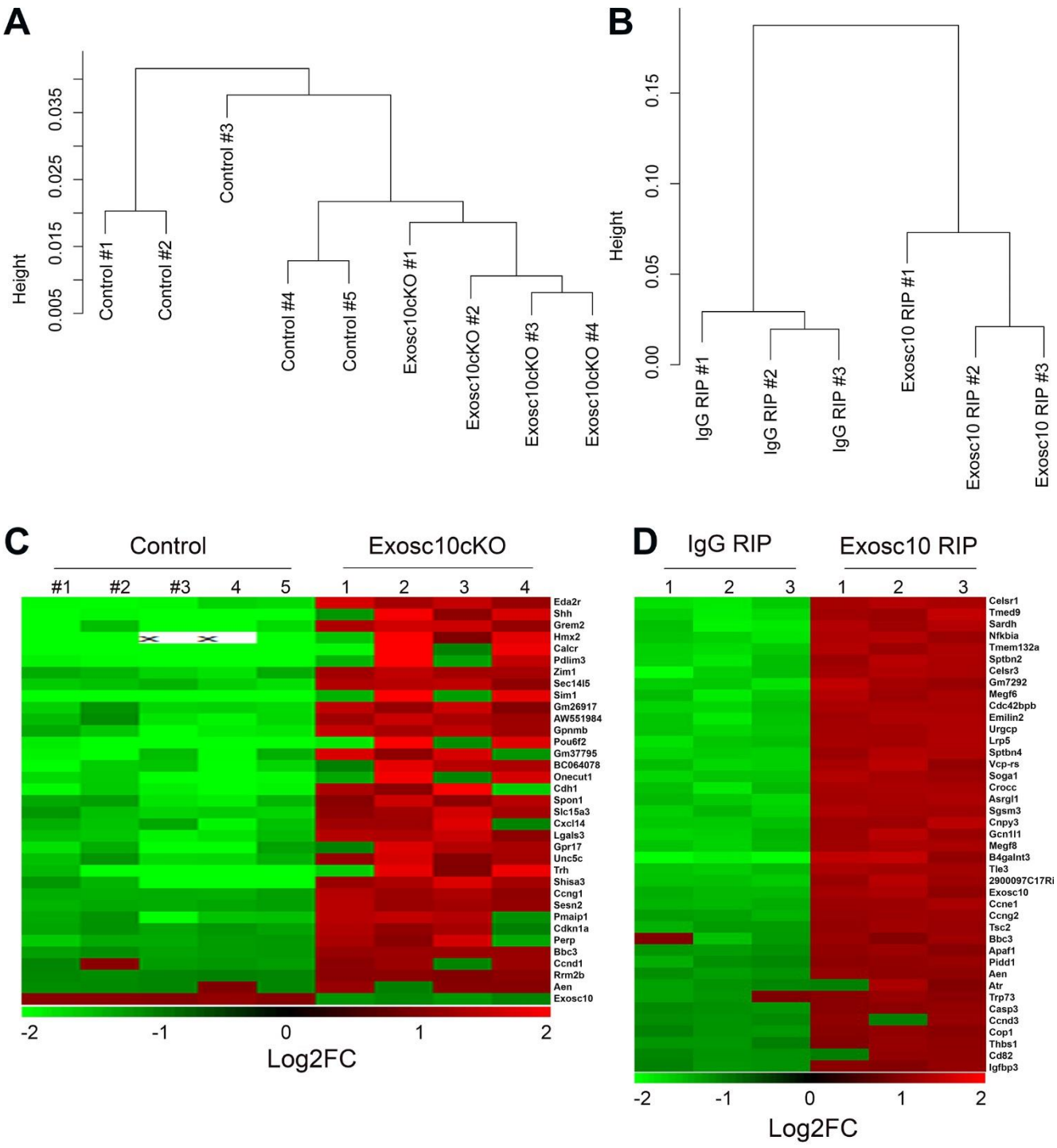

Figure S4. Cluster and Heatmap analyses of RNA-seq and RIP-seq samples.

(A, B) cluster dendrogram analysis of all RNA-seq (A, control, Exosc10cKO) and RIP-seq (B, IgG RIP, Exosc10 RIP) samples. The log2-nomalized values of all the genes were used for cluster analysis. (C, D) Heatmaps showing changes in gene expression (C) and transcript binding enrichment (D) revealed by RNA-seq (E12.5 Exosc10cKO cortex vs. control) and RIP-seq (E12.5 cortex, Exosc10 antibody vs IgG) analyses, respectively. Top 25 upregulated/enriched genes and genes involved in P53 apoptosis signalling were displayed. Additionally, Exosc10 was shown as a control.

Supplementary Figure 5

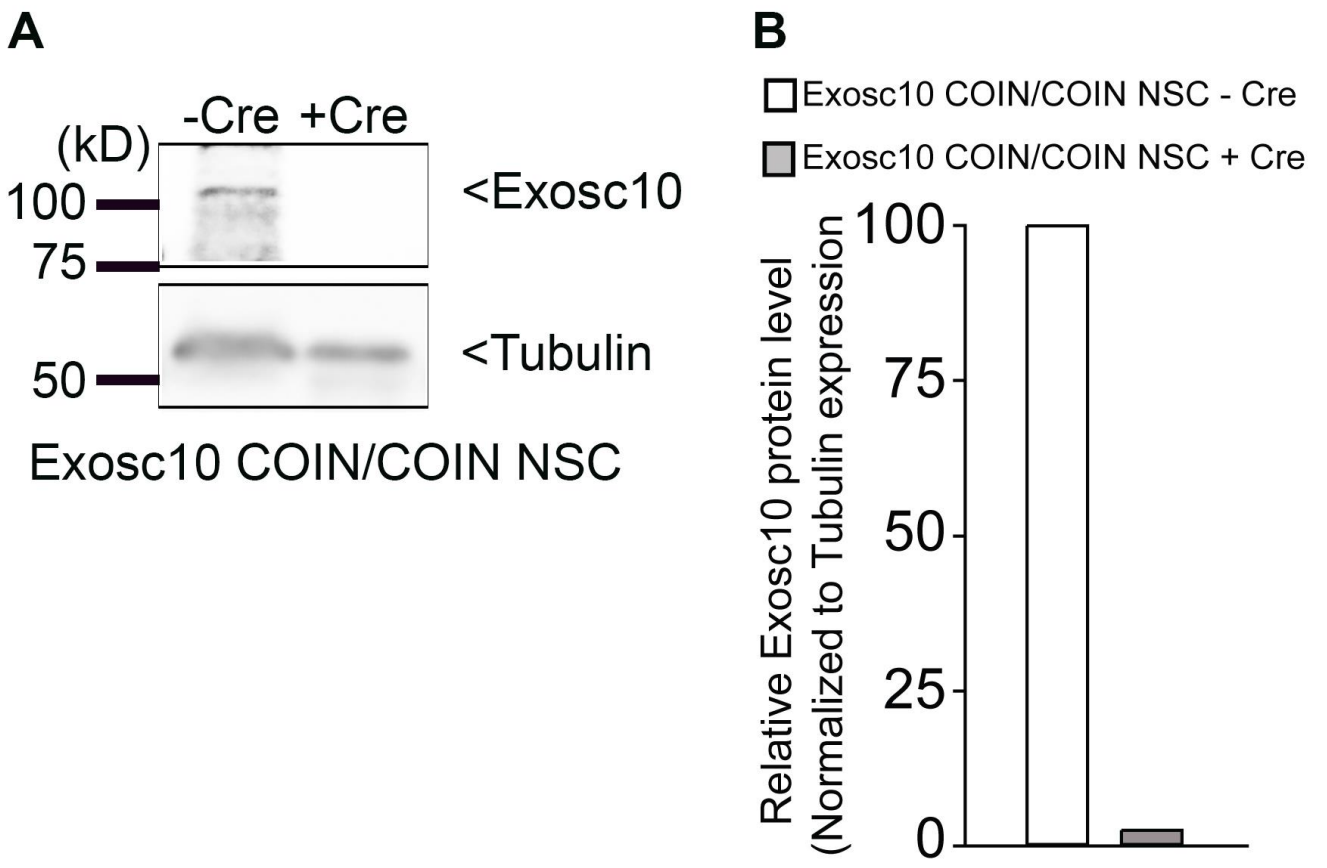

Figure S5. Knockout of Exosc10 using soluble Tat-Cre recombinase in Exosc10$^{COIN/COIN}$ NSCs and the effects of PFTα treatment on Bbc3 expression in the developing cortex.

(A) Western blot (WB) analysis of Exosc10 expression in Exosc10$^{COIN/COIN}$ NSCs without Cre (-Cre) as control and after 26h of treatment with soluble Tat-Cre recombinase (+Cre). Tubulin is shown as a loading control. (B) Quantification of the protein band densities (from A) relative to control (as 100%), which was normalized to tubulin.

Table S1. Genes regulated by Exosc10 in the Exosc10_*Emx1*-Cre cortex at E12.5

Click here to Download Table S1

Table S2. Gene Ontology Categories Significantly Enriched for upregulated genes in E12.5 Exosc10_*Emx1*-Cre cortex Compared with Controls in Expression Analyses

Click here to Download Table S2

Table S3. RIP-seq data for Exosc10 with E12.5 cortex

Click here to Download Table S3

Table S4. Gene Ontology Categories Significantly Enriched for transcripts bound by Exosc10 in RIP-Seq experiment

Click here to Download Table S4

Table S5. Overlap between upregulated genes in RNA-Seq of E12.5 Exosc10cKO cortex and transcripts bound by Exosc10 in RIP-Seq with E12.5 cortex.

Click here to Download Table S5

Table S6. Gene Ontology Categories Significantly Enriched for genes, in which their expression were upregulated in RNA-Seq of E12.5 Exosc10cKO cortex and their transcripts were bound by Exosc10 in RIP-Seq with E12.5 cortex

Click here to Download Table S6

Table S7. Statistical analyses

Click here to Download Table S7

Supplementary Materials and Methods

Antibodies

Polyclonal (pAb) and monoclonal (mAb) primary antibodies used in this study (working dilution; sources): Aen rabbit pAb (1:400; Bioss), Caspase-3 rabbit pAb (1:200; Cell Signaling), Ctip2 rat mAb (1:200; Abcam), Cux1 rabbit pAb (1:50; Santa Cruz), Exosc10 rabbit pAb (1:500 for WB; Proteintech), Exosc10 rabbit pAb (5µg for 100µl RIP-sample; Abcam), GFP chick pAb (1:400; Abcam), HuCD mouse mAb (1:20; Thermo Fisher Scientific), NeuN mouse mAb (1:200, Chemicon), Reelin mouse mAb (1:100), Satb2 mouse mAb (1:200; Abcam), Sox2 mouse mAb (1:100; Santa Cruz), Sox2 rat mAb (1:100; eBioscience), Sox5 rabbit pAb (1:100; Santa Cruz), Tbr1 rabbit pAb (1:300; Abcam), Tbr2 rabbit pAb (1:300; Chemicon), Tbr2 rat mAb (1:200; eBioscience), Tuj mouse mAb (1:500; Chemicon), Pax6 mouse mAb (1:100; Developmental Studies Hybridoma Bank). Secondary antibodies used were Alexa 488-, Alexa 568-, Alexa 594- and Alexa 647-conjugated IgG (various species, 1:400; Molecular Probes).

Relative quantification of cortical size

Relative quantification of cortical size was performed as described previously (Tuoc et al. 2013; Narayanan et al. 2018). Briefly, dorsal views of forebrains of mutant and control mice were photographed under a dissection microscope. Cortical anterior-posterior axis (AP), cortical surface and midline lengths from the digitized images were measured with Fiji software to make comparison between mutants and controls.

Immunohistochemistry (IHC)

IHC was performed as described previously (Tuoc et al. 2009). Briefly, Embryonic and postnatal brains were fixed in 4% paraformaldehyde, incubated in 25% sucrose in PBS-DEPC at 4°C overnight, embedded in Tissue-Tek O.C.T Compound (Sakura Finetek) on dry ice and cut in 8-16 µm coronal sections. After blocking with 5% goat or donkey normal serum, sections

were incubated overnight with primary antibody at 4°C and the signal was detected with a fluorescent secondary antibody (Alexa Fluor; 1:400; Invitrogen). Sections were later counterstained with Vectashield mounting medium containing 4'-6'-diamidino-2-phenylindole (DAPI) (Vector Laboratories) to label nuclei.

Quantitative RT-PCR (qPCR) and Western blot analyses

qRT-PCR and Western blot analyses were performed as described previously (Tuoc and Stoykova 2008b). Primers used for qPCR:

Aen

Forward: 5'-GGCCGGGTTTTCAGATCCTTA-3'
Reverse: 5'- GCTGAGCAGGTTTGGGACAT-3'

Bbc3

Forward: 5'-ACGACCTCAACGCGCAGTA-3'
Reverse: 5'-CTAGTTGGGCTCCATTTCTGG-3'

Atr

Forward: 5'-AGGACACTCCAAAGCACCACTG-3'
Reverse: 5'-GCAGCCCTGTTACTCTATTTCGG-3'

18S

Forward: 5'-CTTAGAGGGACAAGTGGCG-3'
Reverse: 5'-ACGCTGAGCCAGTCAGTGTA-3'

Cell counts and quantitative analysis of IHC signal intensity

IHC quantification was performed using anatomically matched coronal sections. Nucleus marker-positive cells were counted using the Cell Counter plugin of Fiji (Schindelin et al. 2012).

In most cases, cell counts of six matched sections were averaged (control/cKO). The number of lineage marker cells was quantified using the total marker-positive cells in a defined region (radial unit) alone, or by normalizing to the total number of DAPI+ (nucleus-stained) cells using the following equation: Normalized number = marker-positive cell number/DAPI+ cell number. For quantitative analyses of IHC signal intensity of cytoplasm-staining markers, fluorescent images of selected areas of the cortex were used. Color images were converted to gray scale and the fluorescent signal intensity values were measured using the Analyze/Measure function of Fiji software. The signal intensity from the background next to the tissue was subtracted from the measured intensity for normalization. The normalized intensities of cKO sections are displayed relative to normalized values from control experiments as a percentage. Statistical comparisons of histological data were performed using Student's t-test. All bar graphs are plotted as means ± SEM. All statistical tests are two-tailed, and P-values are considered to be significant for $p < 0.05$ ($*p < 0.05$, $**p < 0.01$, and $***p < 0.005$; NS, not significant).

SUPPLEMENTAL REFERENCES

Afgan E, Baker D, Batut B, van den Beek M, Bouvier D, Cech M, Chilton J, Clements D, Coraor N, Gruning BA et al. 2018. The Galaxy platform for accessible, reproducible and collaborative biomedical analyses: 2018 update. *Nucleic Acids Res* **46**: W537-W544.

Chen J, Bardes EE, Aronow BJ, Jegga AG. 2009. ToppGene Suite for gene list enrichment analysis and candidate gene prioritization. *Nucleic acids research* **37**: W305-311.

Huang da W, Sherman BT, Lempicki RA. 2009a. Bioinformatics enrichment tools: paths toward the comprehensive functional analysis of large gene lists. *Nucleic Acids Res* **37**: 1-13.

Kilchert C, Wittmann S, Vasiljeva L. 2016. The regulation and functions of the nuclear RNA exosome complex. *Nat Rev Mol Cell Biol* **17**: 227-239.

Love MI, Huber W, Anders S. 2014. Moderated estimation of fold change and dispersion for RNA-seq data with DESeq2. *Genome biology* **15**: 1.

Narayanan R, Pham L, Kerimoglu C, Watanabe T, Castro Hernandez R, Sokpor G, Ulmke PA, Kiszka KA, Tonchev AB, Rosenbusch J et al. 2018. Chromatin Remodeling BAF155 Subunit Regulates the Genesis of Basal Progenitors in Developing Cortex. *iScience* **4**: 109-126.

Oliveros J. 2007–2015. Venny. An interactive tool for comparing lists with Venn's diagrams.

Schindelin J, Arganda-Carreras I, Frise E, Kaynig V, Longair M, Pietzsch T, Preibisch S, Rueden C, Saalfeld S, Schmid B et al. 2012. Fiji: an open-source platform for biological-image analysis. *Nat Methods* **9**: 676-682.

Tuoc TC, Boretius S, Sansom SN, Pitulescu ME, Frahm J, Livesey FJ, Stoykova A. 2013. Chromatin Regulation by BAF170 Controls Cerebral Cortical Size and Thickness. *Developmental Cell* **25**: 256-269.

Tuoc TC, Radyushkin K, Tonchev AB, Pinon MC, Ashery-Padan R, Molnar Z, Davidoff MS, Stoykova A. 2009. Selective cortical layering abnormalities and behavioral deficits in cortex-specific Pax6 knock-out mice. *Journal of neuroscience* **29**: 8335-8349.

Tuoc TC, Stoykova A. 2008a. Trim11 modulates the function of neurogenic transcription factor Pax6 through ubiquitin-proteosome system. *Genes & development* **22**: 1972-1986.

Visel A, Thaller C, Eichele G. 2004. GenePaint.org: an atlas of gene expression patterns in the mouse embryo. *Nucleic Acids Res* **32**: D552-556.

Wang J, Duncan D, Shi Z, Zhang B. 2013. WEB-based GEne SeT AnaLysis Toolkit (WebGestalt): update 2013. *Nucleic Acids Res* **41**: W77-83.

Wang J, Vasaikar S, Shi Z, Greer M, Zhang B. 2017. WebGestalt 2017: a more comprehensive, powerful, flexible and interactive gene set enrichment analysis toolkit. *Nucleic Acids Res* **45**: W130-W137.

Zhang B, Kirov S, Snoddy J. 2005. WebGestalt: an integrated system for exploring gene sets in various biological contexts. *Nucleic Acids Res* **33**: W741-748.

Zhao C, Teng EM, Summers RG, Jr., Ming GL, Gage FH. 2006. Distinct morphological stages of dentate granule neuron maturation in the adult mouse hippocampus. *J Neurosci* **26**: 3-11.

Macosko EZ, Basu A, Satija R, Nemesh J, Shekhar K, Goldman M, Tirosh I, Bialas AR, Kamitaki N, Martersteck EM et al. 2015. Highly Parallel Genome-wide Expression Profiling of Individual Cells Using Nanoliter Droplets. *Cell* **161**: 1202-1214.

Telley L, Govindan S, Prados J, Stevant I, Nef S, Dermitzakis E, Dayer A, Jabaudon D. 2016. Sequential transcriptional waves direct the differentiation of newborn neurons in the mouse neocortex. *Science* **351**: 1443-1446.